CrossMark

Typhoon Haiyan overwash sediments from Leyte Gulf coastlines show local spatial variations with hybrid storm and tsunami signatures

Janneli Lea A. Soria [a,b], Adam D. Switzer [a,b,*], Jessica E. Pilarczyk [c], Fernando P. Siringan [d], Nicole S. Khan [e], Hermann M. Fritz [f]

[a] Asian School of the Environment, Nanyang Technological University, 639798, Singapore
[b] Earth Observatory of Singapore, Nanyang Technological University, 639798, Singapore
[c] Division of Marine Science, School of Ocean Science and Technology, University of Southern Mississippi, Stennis Space Center, MS 39529, USA
[d] Marine Science Institute, University of the Philippines, Diliman, Quezon City 1101, Philippines
[e] United States Geological Survey, St. Petersburg Coastal and Marine Science Center, St. Petersburg, FL 33701-4846, USA
[f] School of Civil and Environmental Engineering, Georgia Institute of Technology, Atlanta, GA 30332, USA

ARTICLE INFO

ABSTRACT

Marine inundation associated with the 5 to 8 m storm surge of Typhoon Haiyan in 2013 left overwash sediments inland on the coastal plains of the northwestern shores of Leyte Gulf, Philippines. The Haiyan overwash deposit provides a modern sedimentary record of storm surge deposition from a Category 5 landfalling typhoon. We studied overwash sediments at two locations that experienced similar storm surge conditions but represent contrasting sedimentological regimes, namely a siliciclastic coast and a mixed siliciclastic-carbonate coast. The contrasting local geology is significantly reflected in the differences in sediment grain size, composition and sorting at the two sites. The Haiyan overwash sediments are predominantly sand and silt and can be traced up to ~1.6 km inland, extending farther beyond the previously reported <300 m inland limit of sedimentation. Sites with similar geology, topographic relief, and overland flow conditions show significant spatial variability of sediment thickness and inland extent. We infer that other local factors such as small-scale variations in topography and the type of vegetation cover might influence the spatial distribution of overwash sediments. The Haiyan overwash deposits exhibit planar stratification, a coarsening upward sequence, a non-systematic landward fining trend, and a sharp depositional (rarely erosional) basal contact with the underlying substrate. Overall, the Haiyan deposits have sedimentologic and stratigraphic characteristics that show a hybrid signature common to both storm and tsunami deposits.

1. Introduction

Overwash associated with storm surges during landfalling cyclones often rework, erode and transport near-shore sediments onto low-lying coastal plains (e.g., Leatherman, 1981; Morton and Sallenger, 2003; Williams and Flanagan, 2009). The overwash sediments are commonly recognized as anomalous sand layers found in the sedimentary environments of low-energy coastal settings, including coastal lakes, swamps and back barrier tidal marshes (e.g., Leatherman and Williams, 1977; Liu and Fearn, 1993; Buynevich et al., 2004; Donnelly et al., 2004). Overwash processes also create depositional landforms on back beach environments. Depending on the elevation of the water surface level relative to the dune or beach ridge height, along with

the extent and continuity of foredune gaps, overwash can result in washover fans that are isolated or merge to form washover terrace morphology (Morton and Sallenger, 2003).

Similarly, tsunamis also produce overwash and associated deposits. Although the hydrodynamics of a tsunami can be distinctly different from that of a storm surge in terms of overland flow velocity, wave set-up, wave period, and inland extent (e.g., Switzer and Jones, 2008; Goto et al., 2009; Watanabe et al., 2017), the associated overwash sediments often show similar sedimentological characteristics (e.g., Kortekaas, 2002; Kortekaas and Dawson, 2007; Switzer and Jones, 2008). In a few cases, however, multi-proxy approaches using sedimentology, micro-fossils, geochemistry, archaeology, and paleoecology have successfully differentiated a tsunami from a storm deposit in the geologic record (e.g., Nanayama et al., 2000; Goff et al., 2004; Kortekaas and Dawson, 2007; Morton et al., 2007; Ramírez-Herrera et al., 2012). Attributing a deposit to a certain event type, in particular between storm and tsunami, needs careful consideration of the complex interactions between the hydrodynamic processes, the local conditions that determine the

overwash sedimentation patterns, and post-depositional preservation (e.g., Switzer and Jones, 2008; Otvos, 2011).

The Typhoon Haiyan overwash deposit (Table 1) represents a rare modern sedimentary record of an intense landfalling cyclone with a bore-like storm surge. On 8 November 2013, Typhoon Haiyan (Fig. 1) generated a storm surge with a flow depth and inundation distance similar to other recent intense storms such as hurricanes Katrina, Rita, and Ike, and Cyclone Yasi (Table 2). Notably, Typhoon Haiyan's bore-like storm surge is unusual compared to the more commonly reported gradual rise and prolonged inundation associated with comparable storms (Mikami et al., 2016). The deep, high-velocity flow and short inundation duration of Haiyan's storm surge are more commonly attributed to tsunami flooding hydrodynamics (e.g., Morton et al., 2007; Switzer and Jones, 2008) (Tables 3–5). The sedimentary deposit associated with Typhoon Haiyan provides a contrast to the modern storm deposit record, which is dominated by a higher frequency of storm surges characterized by a slower and longer duration of flooding (Table 2).

In this study, we describe the physical sedimentology of overwash sediments resulting from the Typhoon Haiyan storm surge across two nearby coastal plains (Fig. 2a) that have contrasting topographic relief and sedimentological regimes. The Basey coast has irregular topography characterized by raised carbonate platforms and a narrow beach consisting of mixed siliciclastic-carbonate sediments. In contrast, Tanauan is characterized by a broad, subdued coastal plain (<3 m in elevation) that is underlain by siliciclastic sediments. By investigating Haiyan overwash sediments from two nearby sites that experienced similar storm surge characteristics, we are able to evaluate whether local topography and geology has a dominant control on the physical sedimentology and the spatial distribution of overwash sediments. In addition, we compared the Haiyan overwash sediments to those from recent storms such as hurricanes Katrina, Rita, Ike, and Yasi (Table 2) and tsunamis such as the 2011 Tohoku, 2006 West Java, and 2004 Indian Ocean (Tables 3–5) to determine the influence of the bore-like inundation to the physical characteristics and distribution of the Haiyan deposit.

2. Typhoon Haiyan

Typhoon Haiyan, locally known as Yolanda, was a Category 5 typhoon according to the Saffir-Simpson Hurricane Scale when it made landfall on Leyte Island (Fig. 1). Typhoon Haiyan ranks as the most intense and fastest moving storm at landfall worldwide (Lin et al., 2014; Takagi and Esteban, 2016). The areas surrounding San Pedro Bay in Leyte Gulf experienced the most extensive infrastructure damage and highest death toll from Typhoon Haiyan due to the high storm surge and superimposed storm waves (e.g., Morgerman, 2014; Tajima et al., 2014; Mas et al., 2015). The storm surge in San Pedro Bay was initially characterized by a sea-level drawdown of ~2 m that exposed wide expanses of the gently sloping subtidal sand flats along the northern shores of the bay (Soria et al., 2016). Soon after Typhoon Haiyan's landfall on Leyte Island, the storm surge came rapidly onshore as a fast-moving wall of water exceeding 5 m in height (Supplementary Fig. S1). Wave contributions raised high-water mark indicators to almost 8 m in Tacloban and Palo (Soria et al., 2016). The peak water levels lasted for 30 to 45 min before receding within 1 to 2 h (e.g., Morgerman, 2014; Soria et al., 2016). The inundation duration was short, but involved three wave sets based on corroborated survivor accounts and storm surge simulations (Soria et al., 2016). On the northern shore of San Pedro Bay, storm surge flooding at Basey reached ~800 m inland, whereas on the western shore near Tanauan, flooding reached up to 2 km inland. The coastal inundation caused shoreline changes, including beach erosion and inland sedimentation (Supplementary Figs. S2–S4). Beach scouring and exposed tree roots following Typhoon Haiyan clearly indicate beach erosion at several locations around Leyte Gulf (Supplementary Figs. S3a–c, S4a–b). Conversely, the

washover terrace that was formed along the Tanauan coast illustrates inland sedimentation (Supplementary Fig. S2b–c).

3. Study area

San Pedro Bay is a ~20 km wide by ~25 km long embayment that opens to the larger Leyte Gulf to the south (Fig. 1 inset). To the northwest, San Pedro Bay narrows into the San Juanico Strait that separates the islands of Leyte and Samar. San Pedro Bay is relatively shallow (maximum water depth of ~20 m, average water depth of ~10 m) and has a tidal range of 0.5 m (PMSL, 2016).

We focused our study on two locations in San Pedro Bay that represent contrasting coastal morphology and geology (Fig. 2a). The irregularly steep karstic terrain of the Oligocene to Miocene age limestones (Aurelio and Peña, 2002) occurs on the northern and eastern shores of San Pedro Bay in the area of Basey (Fig. 2a, c). Here, the rocky limestone headlands bound small embayments with sandy pocket beaches and are surrounded by narrow fringing reefs (Fig. 2c). In contrast, the western coast of Leyte between Tacloban and Tanauan is characterized by a wide, low elevation (<3 m) coastal plain that consists of beach ridges, a sand spit and patches of mangrove stands (Fig. 2d). The coastal plains consist primarily of accumulations of unconsolidated siliciclastic sediments sourced from the interior highlands that are composed of Cretaceous ultramafic-mafic igneous rocks capped with pelagic sedimentary sequences and patches of Miocene-Pliocene volcanic centers and sedimentary rocks (Aurelio and Peña, 2002; Suerte et al., 2005).

4. Methods

4.1. Transect-scale sampling

The inland distribution of sediments from Typhoon Haiyan were mapped along the coastline of San Pedro Bay in January 2014 along four transects at two locations that represent contrasting depositional regimes (Fig. 2a). One transect (Ba) was located on the mixed carbonate-siliciclastic coast of Basey (Fig. 2c) and three transects (Sc, So and Ma) were located on the siliciclastic coast of Tanauan (Fig. 2d). Each transect extended from the shore to the landward limit of the Haiyan deposit, the inland extent varied from 400 m in Basey to 1.8 km in Tanauan. The transects cover back beach environments, including stands of *Nypa fruticans* (a mangrove-associated palm species), patches of grassland, coconut groves, and rice fields. We sampled the Haiyan deposit along each transect using a hand gouge auger down to a depth of ~20 cm or by a shovel down to depths of ~10 cm. In total we collected samples at 44 sites: one sediment sample from the Typhoon Haiyan deposit and one sample from the underlying soil (not sampled in So 1–6). We used a handheld GPS to mark all the sampling locations and focused our study on the overwash deposits from back beach environments, which were minimally influenced by marine processes after the storm. Our surveys were limited to areas that were accessible and had minimal disturbance from retrieval operations and rehabilitation efforts following Typhoon Haiyan, which resulted in sampling points that were patchy and at irregular distances. The transects correspond to those defined in the micropaleontological study of Pilarczyk et al. (2016). Based on the micropaleontological assemblages contained within the Typhoon Haiyan overwash sediments, Pilarczyk et al. (2016) established a nearshore to offshore sediment source for the Haiyan deposit.

4.2. Trench-scale sampling

For a detailed description of the sedimentary features of the Haiyan deposits, a follow-up field survey was conducted in May 2014. An array of seven shallow trenches were excavated in two transects oriented perpendicular to the coast (Fig. 2b), starting

Table 1

Comparison of the hydrodynamics and sedimentary signatures of the Typhoon Haiyan storm surge in Leyte Gulf.

		Tanauan, Leyte	Basey, Samar	Tanauan, Leyte	Tolosa, Leyte	Tolosa, Leyte
Local setting	Locality					
	Coastal geomorphology	Sandy beach, coastal plain	Narrow sandy beach on carbonate platform	Sandy beach	Sandy beach	Beach–ridge plain
	Ground surface elevation, m (asl)	1.5 to 2m	2 to 3m	0 to 5m	0 to 3m	0 to 2.5 m
Hydrodynamic conditions	Flow depth, m	3 to 4m	3 to 4m	3.6 m	3.8 m	3.5 m
	Inundation distance, km	2 km	0.8 km	3.1 km	1.4 km	0.8 km
	Distance from storm eye (zone of max winds)*	15 km	30 km	15 km	5 km	5 km
	References	Soria et al., 2016	Soria et al., 2016	Abe et al., 2015	Abe et al., 2015	Brill et al., 2016
Sedimentary textures and structures / **Trench scale**	Thickness	10–20cm (proximal); 2cm (distal)	2 to 8cm	0.1 cm to 10 cm; 40 to 80 cm very close to shore	0.1 cm to 10 cm	10 to 20 cm (proximal); few mm, 2 to 5 cm (distal)
	Vertical grading of entire deposit	Unit 1 (sand sheet to mud): coarsening upward. Unit 2 (washover terrace): coupled fining and coarsening upward	No analysis	No analysis	No analysis	Unit 1 (sandsheet): fining upward. Unit 2 (washover terrace): repeated coarsening fining sequences
	Sorting	Moderate to well–sorted	Poorly sorted	No analysis	No analysis	Well–sorted
	Sedimentary structures	Unit 1: massive to horizontal planar lamination. Unit 2: subhorizontal planar laminae	Massive	No analysis	No analysis	Unit 1: planar lamination; scour marks at the base. Unit 2: inclined lamination (10–15º)
	Basal contact	Sharp, depositional	Sharp, depositional	No analysis	No analysis	Sharp, erosional and depositional
Transect scale	Cross–shore geometry	Washover terrace (proximal); sand sheet to mud (distal) with varying thickness landwards but generally thick in depressions	Overall but not systematic landward thinning	Landward thinning	Landward thinning	Washover terrace (proximal); sand sheet (distal) exhibiting landward thinning
	Lateral grading	Overall landward fining	Overall landward fining	No analysis	No analysis	Landward fining
	Inland extent	1.6 km	350 m	150 m to 80 m (sandsheet)	130 m to 150 m (sandsheet)	250 m (sandsheet)
	References	This Study	This Study	Abe et al., 2015	Abe et al., 2015	Brill et al., 2016

* Estimated based on the storm eye location of Morgerman, 2014.

from the terminus of a sandy landform identified on the post-typhoon Haiyan satellite image to about 100 m landward (Fig. S2b, c). The trenches were located on a shallow grass-covered depression adjacent to transect Ma that, at the time of the initial survey, had ponded water about 50 cm deep (Fig. 2b). The trench samples were labelled as MP to distinguish them from the samples taken using an auger along transect Ma. The trenches have varying depths depending on the position of the water table and ranged from 25 to 50 cm below the surface. At each trench, we noted the thickness of the Haiyan deposit, the nature of the basal contact with the underlying land surface, and other sedimentary structures such as laminations or apparent grading. Samples from the Haiyan deposit and the pre-Haiyan soil were taken at 2-cm intervals for subsequent sedimentologic analyses.

4.3. Surveying

All sample sites were surveyed and topographic elevations along the transects were determined simultaneously with a Haiyan high-water mark survey in January 2014 (Soria et al., 2016) using a differential Trimble global positioning system (dGPS) rover connected via Bluetooth to a Lasercraft XLRic laser range finder (Fritz et al., 2012; Soria et al., 2016). The elevation measurements were differentially corrected with our daily setup of the local Ashtech™ base station and corrected for tide level at the time of the survey on the basis of tide predictions provided by XTide 2© open-source software of Flater (1998). The typhoon-damaged tide station in Tacloban Port was visited during the survey and reference points were surveyed to align the vertical datum with mean sea level at the local tide station. The tide recordings for Tacloban Port were provided by the National Mapping and Resources Information Agency (NAMRIA) of the Republic of the Philippines. The post-processed differentially corrected position and elevation measurements with respect to MSL have an individual confidence of ±0.1 m.

4.4. Sedimentologic analyses

4.4.1. Organic matter and carbonate content

About 1 to 2 g of sediment was subsampled from each sample to determine both the organic matter and carbonate content following the loss-on-ignition method (Dean, 1974; Heiri et al., 2001). The sediments were placed in pre-weighed ceramic crucibles that were dried in an oven at 105 °C for up to 2 h (Dean, 1974). The samples and crucibles were allowed to cool to room temperature, and then were weighed to obtain the initial dry weight of the sediments. The samples in crucibles were sequentially heated in a muffle furnace, first at 550 °C for 4 h to burn the organic matter component, and then at 950 °C for 1 h to burn the carbonate component (Heiri et al., 2001). After each heating stage, the samples were allowed to cool at room temperature and then weighed. The weight lost from the initial dry weight at each heating stage corresponds accordingly to the relative organic matter and carbonate content. We followed the calculations given by Heiri et al. (2001) to determine the relative amounts of organic matter and carbonate component.

4.4.2. Grain size distribution

We used two different optical techniques with similar grain size measuring principles to determine the sediment grain size distribution of the samples. After visually estimating the modal and maximum grain size using a grain size chart comparator, fine-grained sediments (<2 mm diameter) were subjected to laser diffraction particle size analysis with a Malvern Mastersizer 2000, whereas coarse-grained sediments (>2 mm diameter) were subjected to digital imaging using a Retsch Technology Camsizer®. The Camsizer can measure grain size, which corresponds to the cross-sectional area of the particles in the image and is reported as the diameter of a circle of equivalent area, which is similar to the grain size measuring principle of the laser particle analyzer (Switzer and Pile, 2015). A total of 141 samples composed mostly of mud to fine sand, including all the samples taken from the
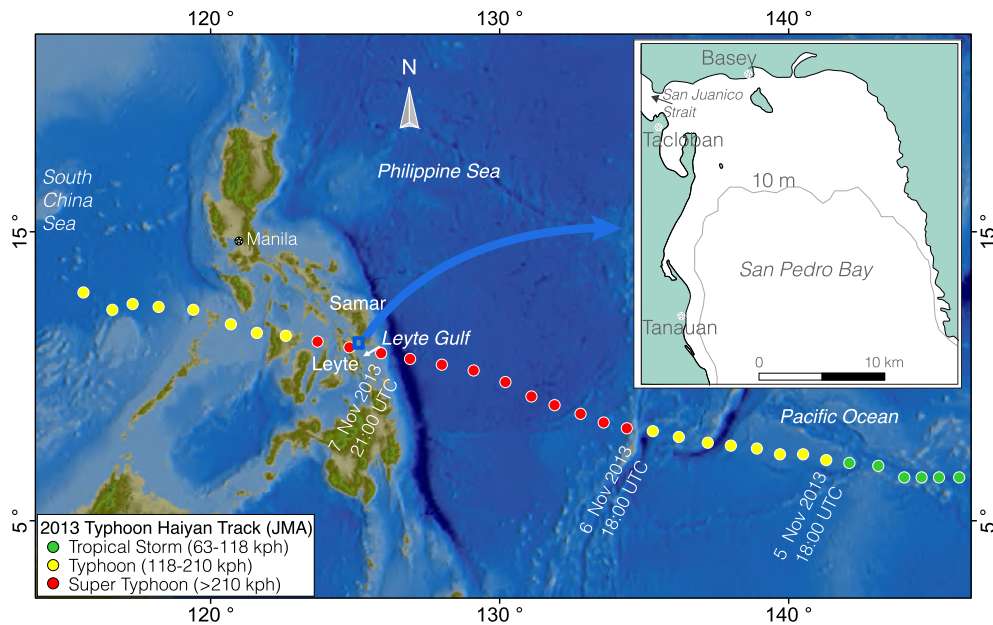
Fig. 1. Study area. Track of Typhoon Haiyan traversing central Philippines in November 2013. Inset: San Pedro Bay and surrounding coastal towns including Basey and Tanauan.

four transects (Ba, Sc, So and Ma), all samples from the three trenches (MP 1,2,5), and the pre-Haiyan soil samples in four trenches (MP 3,4,6,7), were analysed using the Malvern Mastersizer. In contrast, 28 samples corresponding to the Typhoon Haiyan deposit from trenches MP3, MP4, MP6, and MP7, which are predominantly sand and contain granules, were analysed using the Camsizer. For the samples that were introduced to the Malvern Mastersizer, ~1 g of sediment was treated with 15% H_2O_2 to remove organics and 10% hydrochloric acid (HCl) to remove carbonate fragments. The samples were rinsed with distilled water before conducting the grain size analysis using laser diffraction.

For the coarse sand Typhoon Haiyan deposits that were analysed using the Camsizer, any organic debris and carbonate fragments that were large enough to be seen with the naked eye were manually removed using forceps instead of being dissolved in chemicals. The sediments were rinsed with distilled water to remove salts, enhancing sediment dispersion. The sediments were successively oven dried at 50 °C, and about 50 to 100 g of dry subsamples were introduced on the Retsch Technology CAMSIZER® for grainsize analyses. We note that the mixed siliciclastic-carbonate sediments of Basey (i.e., LOI > 10% carbonate) were not treated with HCl. Acid treatment biases the inherent bulk sediment composition and preferentially removes the carbonate grains, which may introduce artefacts in the granulometric parameters that are usually used in discriminating an overwash deposit from the background soil (e.g., Szczuciński et al., 2012; Gouramanis et al., 2017).

The grain size data were collectively run through the open-source program GRADISTAT version 8.0 (Blott and Pye, 2001) to generate statistical grain size distributions. The fraction of sediment within each size category (e.g., clay, very coarse silt, medium sand) along with the logarithmic (Folk and Ward, 1957) mean, median, mode, sorting, and skewness of each sample were used to establish the vertical and spatial variations of the Haiyan deposits. All sediment distribution results are listed in Supplementary Tables S1–S11.

5. Results

5.1. Haiyan overwash sediments from Basey

In the field, the Haiyan overwash sediments from Basey were distinguished from the pre-Haiyan soil by color. The stratigraphic contact between the overwash sediments and the underlying layer varied in degree of prominence depending on the coastal environment and distance from the shore. The Haiyan sediments in the coconut grove within 200 m from the shore are grey (10YR 6/1) and overlie very dark grey (10YR 3/1), organic-rich, finer-grained pre-Haiyan soil (Fig. 3a). In the coconut grove, the nature of the contact between the Haiyan sediments and the underlying soil was generally sharp and very pronounced. Farther inland on the rice paddies, the grey (10YR 5/1) Haiyan sediments overlie a mottled grey (10YR5/1) and brown (10YR 4/3) pre-Haiyan agricultural soil (Fig. 3b), but the stratigraphic contact is less discernable.

We observed spatial variations in deposit thickness, grain size, sorting, skewness, and composition (Fig. 4). The Haiyan overwash sediments consist of silt to fine sand that drapes the beach berm, coconut grove and rice paddies on the coastal plain nearly 350 m from the shore (Fig. 4i). The thickest deposit was ~8 cm and was found 30 m from the shore (Fig. 4ii). The Haiyan deposit thins rapidly landward of the shoreline and varies in thickness from 1 to 4 cm. Except for Ba15 and Ba13, the Haiyan sediments deposited on the berm and coconut grove were coarser (very fine to medium sand, Fig. 4iii), better sorted (1 to 2 ϕ, Fig. 4iv), and more finely skewed (0.1 to 0.6 ϕ, Fig. 4v), compared to the sediments deposited on the rice paddies farther inland which are silt-size (Fig. 4iii), very poorly sorted (>2 ϕ, Fig. 4iv), and coarse skewed (−0.1 to 0.1 ϕ, Fig. 4v). With the exception of one sample, Ba8, the sediments closer to the shore also contained ~10% organic matter, whereas the sediments from the rice paddies contained 15% to 20% organic matter (Fig. 4vi). The Typhoon Haiyan deposits within ~200 m from the shore contain >10% carbonate, but sediments beyond 200 m consistently contain low amounts of carbonate ranging from ~3% to 8% (Fig. 4vii).

5.2. Haiyan overwash sediments from Tanauan

5.2.1. Transect-scale investigations

Similar to Basey, the stratigraphic contact between the Haiyan overwash sediments and the pre-Haiyan soil in Tanauan is defined by color, but exhibits varying degrees of prominence. In the *Nypa* forest and grasslands within 200 m of the shore, the contact between the Haiyan overwash sediments and the underlying soil was pronounced (Fig. 3c). The Haiyan overwash sediments are grey (10YR 5/1) and distinctly different from the very dark brown (10YR 2/2)

Table 2
Comparison of the hydrodynamics and sedimentary signatures of the Typhoon Haiyan storm surge and other recent storms of comparable intensity.

	Tropical cyclone ID	Typhoon Haiyan	Typhoon Haiyan	Cyclone Yasi	Hurricane Ike	Hurricane Ike	Hurricane Rita	Hurricane Katrina	Hurricane Isabel	Hurricane Carla
Storm surge	Event Date	November 2013	November 2013	February 2011	September 2008	September 2008	September 2005	August 2005	September 2003	September 1961
Local setting	Locality	Tanauan, Leyte	Basey, Samar	South of Cairns, northeast Queensland, Australia	Galveston and San Luis Islands, Texas	McFaddin National Wildlife Refuge, Texas	Constance Beach, Louisiana	Ocean Spring and St. Andrews, Mississsippi	Hatteras Is., North Carolina	Matagorda Peninsula, Texas
	Coastal geomorphology	Sandy beach, coastal plain	Sandy beach	Sandy beach ridge plains	Barrier islands (ridge and swale topography)	Palustrine marshes and brackish lakes, sandy beach with low foredunes	Beach ridges separated by low–lying, muddy marshes	Salt marsh	Barrier island with dunes	Barrier island
	Ground surface elevation, m (asl)	1.5 to 2 m	2 to 3 m	Ridge crests at higher than 4 to 5 m	0.75 to 2.2 m	1 to 2 m	0.5 to 1 m (ridges)	1.7 to 5 m	Dunes at 3 to 4 m	
Meteorology	Peak Intensity	Cat 5 (895 hPa; ~314 kph)	Cat 5 (895 hPa; ~314 kph)	Cat 5 (929 hPa ~205 kph)	Cat 4 (231 kph)	Cat 4 (231 kph)	Cat 5 (897 hPa; 288 kph)	Cat 5 (902 hPa; 280 kph)	Cat 4 (> 270 kph)	Cat 5 (280 kph)
	Intensity at landfall	Cat 5 (~296 kph)	Cat 5 (~296 kph)	Cat 5	Cat 2 (175 kph)	Cat 2 (175 kph)	Cat 3 (190 kph)	Cat 3 (920 hPa; 200 kph)	Cat 2	Cat 5 (280 kph)
	Translation speed	41 kph	41 kph		20 kph	20 kph	19 kph	24 kph		
	References	Takagi et al., 2015	Takagi et al., 2015	Boughton et al., 2011	Doran et al., 2009; Morton & Barras, 2011	Doran et al., 2009; Morton & Barras, 2011	Williams, 2009; Morton & Barras, 2011	Morton & Barras, 2011	Morton et al., 2007	Morton et al., 2007
Hydrodynamic conditions	Maximum water level, m (asl)	5 to 6 m	5 to 6 m	3 to 6 m	3–4 m	> 3 m	4 to 5 m	~7 m	2.7 m (open–coast) > 3 m to 4 m	3 to 4 m
	Flow depth, m (above ground surface)	3 to 4 m	3 to 4 m		1 to 4 m		At least 3 m	5 to 6 m	1.26 m (landward limit overwash deposition)	1 to 1.5 m
	Inundation duration	~ 1 hour	~ 1 hour	12 hrs (peak inundation lasting for 2 hrs)	2 days of flooding	2 days of flooding	6 hours	~ 24 hrs	9 hrs (with peak inundation lasting for 5 hrs)	24 hrs
	Inundation distance	2 km	800 m	500 m		25 km		725 to 780 m (< 1 km)	15 to 30 km	15 to 35 km
	Distance from storm eye (zone of max winds)	15 km	30 km	20–40 km	25 to 50 km	~70 km	35 km	40–50 km	55 km	60 km
	References	Soria et al., 2016	Soria et al., 2016	Boughton et al., 2011; Nott et al., 2013	Hawkes and Horton, 2012; Doran et al., 2009	Williams, 2010; Doran et al., 2009	Williams, 2009; McGee et al., 2013	Fritz et al., 2007; Horton et al., 2009	Morton et al., 2007	Morton et al., 2007
Sedimentary textures and structures — Trench scale	Thickness	2 cm (distal) 10–20 cm (proximal)	2 to 8 cm	5 cm (87 m from shore); 20–50 cm (50 m from the shore)	2 cm to 28 cm	51–64 cm (within 200 m); 3–10 cm (> 200 m)	2 to 50 cm	9 to 13 cm	40–97 cm (2 m thick overwash terrace)	At least 25 to 30 cm
	Vertical grading of entire deposit	Unit 1 (sand sheet to mud): coarsening upward Unit 2 (washover terrace): coupled fining and coarsening upward	No analysis	Fining upward with fine–skewed trends	Coarsening upward; alternate coarsening and fining upwards	No analysis	Unit A (sand sheet): coarsening upward Unit B (washover terrace): coarsening upward	Massive	Cycles of upward coarsening or upward fining	Upward fining
	Sorting	Moderate to well–sorted	Poorly sorted	Not reported	Not reported	Not reported	Well sorted	Not reported	Well sorted	Poorly sorted (proximal) to well sorted (distal)
	Sedimentary structures	Unit 1: massive to horizontal planar laminae Unit 2: subhorizontal planar laminae	Massive	Horizontal planar laminations; basal coarse grained sediments	Not reported	Ripple marks on the surface	Unit A: planar laminae Unit B: foreset laminae	Not indicated	Subhorizontal planar stratification	Planar parallel laminae
	Basal contact	Sharp, depositional	Sharp, depositional	Sharp ,erosional	Sharp, depositional with little or no erosion	Sharp	Sharp, erosional	Sharp, erosional	Sharp	Sharp, erosional and depositional
Sedimentary textures and structures — Transect scale	Cross–shore geometry	Washover terrace (proximal); sand sheet to mud (distal) with varying thickness landwards but generally thick in depressions	Overall but not systematic landward thinning	Highly variable thickness	Landward thinning; thicker deposits on the swales	Fining and thinning landward	Landward thinning	No transect data	Narrow thick terrace deposits terminating in avalanche faces	Narrow thick terrace deposits, moderately thin broad fans, landward thinning
	Lateral grading	Overall landward fining	Overall landward fining	Landward fining in one site, no systematic trend in another site	Not reported	Thinning and fining inland	Inland fining only on the distal deposit			Landward fining
	Inland extent	1.6 km	350 m	Up to 87 m	110 to 320 m	2700 m	400 to 500 m		Up to 250 m	Average at 193 m, up to 930 m
	References	This Study	This Study	Nott et al., 2013	Hawkes and Horton, 2012	Williams, 2010	Williams, 2009	Horton et al., 2009	Morton et al., 2007	Morton et al., 2007

Table 3
Comparison of the hydrodynamics and sedimentary signatures of the Typhoon Haiyan storm surge, and two recent tsunami deposits from the 2011 Japan tsunami, and the 2006 Indonesia tsunami.

	Inundation events	2013 Typhoon Haiyan storm surge		2011 Tohoku–oki Tsunami		2006 Western Java Tsunami
Local setting	Locality	Tanauan, Leyte	Basey, Samar	Sendai Plain	Arahama coast, Sendai Plain	Adipala, central Java, Indonesia
	Coastal geomorphology	Sandy beach, coastal plain	Narrow sandy beach on carbonate platform	Sandy beach ridge and swales; with coastal dikes	Coastal lowland with beach ridges	Beach ridge–swale plain
	Ground surface elevation, m (asl)	1.5 to 2 m	2 to 3 m	< 5 m	0 to 3 m	0.5 to 7 m
Hydrodynamic conditions	Maximum surge height or tsunami height, m (asl)	5 to 6 m	5 to 6 m	6 to 20 m	10 m	
	Flow depth, m (above ground surface)	3 to 4 m	3 to 4 m	2 to 6 m	5 m	5 m
	Inundation duration, hour	~ 1 h	~ 1 h	14 significant waves offshore with coastal flooding lasting for at least 3 h**		
	Inundation distance, km	2 km	0.8 km	0.6 to 4 km	4 km	0.75 km
	Water Velocity, m/s	3 to 4 m/s*		~2m/s (2 km from the coast); 6 to 8 m/s (within 1 km)***		
	References	Soria et al., 2016 *Ramos et al., 2014	Soria et al., 2016	Abe et al., 2012 **Sugawara & Goto, 2012	Takashimizu et al., 2012; ***Hayashi & Koshimura, 2012	Moore et al., 2011
Sedimentary textures and structures — **Trench scale**	Thickness	2 cm (distal) 10–20 cm (proximal)	2 to 8 cm	10 to 40 cm (1 to 2 km from the shore); sub–mm to 5 cm (> 2 km)	< 10 cm	10 to 20 cm (70 m from shoreline), 1 mm to 1.5 cm (> 300 m)
	Vertical grading of entire deposit	Unit 1 (sand sheet to mud): coarsening upward Unit 2 (washover terrace): coupled fining and coarsening upward	No analysis	Sand–dominated base capped by mud layer	Normal grading	Coarsening then fining upward in 2 distinct pulses
	Sorting	Moderate to well–sorted	Poorly sorted	Not reported	Poor to moderately sorted	Poor to moderately sorted
	Sedimentary structures	Unit 1: massive to horizontal planar lamination Unit 2: subhorizontal planar laminae	Massive	Mostly massive, at some sites parallel laminae and rip–up clasts are present	Massive sand, parallel laminae, rip–up clasts	Planar laminae
	Basal contact	Sharp, depositional	Sharp, depositional	Sharp, rip–up clasts indicates erosion	Sharp, erosional	Sharp, minimal erosion
Transect scale	Cross–shore geometry	Washover terrace (proximal); sand sheet to mud (distal) with varying thickness landwards but generally thick in depressions	Overall but not systematic landward thinning	Landward thinning	Overall but not systematic landward thinning	Overall but not systematic landward thinning (thickest within 300 m from shore)
	Lateral grading	Overall landward fining	Overall landward fining	Sand–dominated (up to 2 km); mud–dominated (> 2 km)	Landward fining	Overall landward fining
	Inland extent	1.6 km	350 m	600 m to 4 km	~4 km	720 m
	References	This Study	This Study	Abe et al., 2012	Takashimizu et al., 2012	Moore et al., 2011

*, **, *** denote corresponding references.

Table 4
Comparison of the hydrodynamics and sedimentary signatures of the Typhoon Haiyan storm surge and the 2004 Indian Ocean tsunami in Indonesia, Malaysia, India, and Sri Lanka.

	Inundation events	2013 Typhoon Haiyan storm surge		2004 Indian Ocean Tsunami				
		Tanauan, Leyte	Basey, Samar	Banda Aceh, Indonesia	Langkawi, Malaysia	Penang, Malaysia	Kalpakkam and Nagipattinam, Southeast India	Yala, Sri Lanka
Local setting	Locality	Tanauan, Leyte	Basey, Samar	Banda Aceh, Indonesia	Langkawi, Malaysia	Penang, Malaysia	Kalpakkam and Nagipattinam, Southeast India	Yala, Sri Lanka
	Coastal geomorphology	Sandy beach, coastal plain	Narrow sandy beach on carbonate platform	Narrow beaches bounded by headlands	Narrow, steep beach with intertidal zone	Narrow, steep beach with intertidal zone	Narrow beaches with coastal dunes	Narrow sandy beaches bounded by sand dunes
	Ground surface elevation, m (asl)	1.5 to 2 m	2 to 3 m	4 to 35 m	0.1 to 3 m	0.5 to 3 m	< 5 m	0 to 4.5 m
Hydrodynamic conditions	Maximum surge height or tsunami height, m (asl)	5 to 6 m	5 to 6 m		4 m	2 m	6.5 to 11 m	5 m
	Flow depth, m (above ground surface)	3 to 4 m	3 to 4 m	> 25 m			2 to 4 m	4–5 m
	Inundation duration, hour	~ 1 h	~ 1 h		1h:40m		3 waves at 5–min interval in Kalpakkam coast	
	Inundation distance, km	2 km	0.8 km	0.45 km	0.25 km	1.5 km	0.03 to 0.85 km	0.9 km
	Water Velocity, m/s	3 to 4 m/s*		10 m/s			> 3 m/s	
	References	Soria et al., 2016 *Ramos et al., 2014	Soria et al., 2016	Moore et al., 2006	Hawkes et al., 2007 **Bird et al., 2007	Hawkes et al., 2007	Srinivasalu et al., 2007 Switzer et al., 2012	Morton et al., 2008
Sedimentary textures and structures — Trench scale	Thickness	2 cm (distal) 10–20 cm (proximal)	2 to 8 cm	5 to 20 cm (within 50 to 400 m from the beach)	23 cm	15 cm	> 10 cm to 40 cm	20 cm (within 150 m from beach) highly variable 2.5 to 22 cm (> 150 m)
	Vertical grading of entire deposit	Unit 1 (sand sheet to mud): coarsening upward Unit 2 (washover terrace): coupled fining and coarsening upward	No analysis	Massive units exhibiting normal grading	1 fining upward sequence	Coarsening upward sequence	Massive but graded units, coarsening and fining upward; dominantly fining upward in Kalpakkam	Overall but not systematic fining upward
	Sorting	Moderate to well–sorted	Poorly sorted	Poorly sorted	Not reported	Not reported	Poor to well–sorted, mostly moderately sorted	Poor to moderately sorted
	Sedimentary structures	Unit 1: massive to horizontal planar lamination Unit 2: subhorizontal planar laminae	Massive	Palanr lamination, with 1 section exhibiting cross–stratification	Contain shell fragments		Parallel lamination on the basal unit, massive middle unit, and complex bedding such as cross lamination and micro bars on the uppermost unit	Planar, horizontal to subhorizontal laminae
	Basal contact	Sharp, depositional	Sharp, depositional	Sharp, minimal erosion	Sharp	Sharp	Sharp	Sharp, erosional
Transect scale	Cross–shore geometry	Washover terrace (proximal); sand sheet to mud (distal) with varying thickness landwards but generally thick in depressions	Overall but not systematic landward thinning	Sand deposition started at 50 m to 200 m from the beach, thick on topographic lows			Kalpakkam: variable thickness and can be patchy near the the coast then tapers inland to nearly tabular; Nagipattinam: landward thinning	Overall but not systematic landward thinning, thick deposits in topographic lows
	Lateral grading	Overall landward fining	Overall landward fining	Landward fining			Landward fining	Highly variable no predominant pattern; either coarsening or fining
	Inland extent	1.6 km	350 m	400 m			350 m	400 m
	References	This Study	This Study	Moore et al., 2006	Hawkes et al., 2007	Hawkes et al., 2007	Srinivasalu et al., 2007 Switzer et al., 2012	Morton et al., 2008

*, ** denote corresponding references.

Table 5
Comparison of the hydrodynamics and sedimentary signatures of the Typhoon Haiyan storm surge and the 2004 Indian Ocean tsunami in Thailand.

	Inundation Events	2013 Typhoon Haiyan storm surge		2004 Indian Ocean Tsunami				
Local Setting	Locality	Tanauan, Leyte	Basey, Samar	Nam Khem and Khao Lak, Thailand	Phra Thong Island, Thailand	Khao Lak, Thailand	Phi Phi Don, Thailand	Koh Lanta, Thailand
	Coastal geomorphology	Sandy beach, coastal plain	Narrow sandy beach on carbonate platform	Low–lying narrow coastal plain	Beach–ridge plain	Pocket beach in between limestone headlands	Pocket beach in between limestone headlands	Pocket beach in between limestone headlands
	Ground surface elevation, m (asl)	1.5 to 2 m	2 to 3 m	4 to 5 m		< 7 m	0.2 to 4 m	0.1 to 3 m
Hydrodynamic conditions	Maximum surge height or tsunami height, m (asl)	5 to 6 m	5 to 6 m	6 to 10 m	20 m	8 m	9 m	6 m
	Flow depth, m (above ground surface)	3 to 4 m	3 to 4 m	2 m to 6 m				4 m to 5 m
	Inundation duration, hour	~ 1 h	~ 1 h					
	Inundation distance, km	2 km	0.8 km		2 km	1 km to 2 km	0.46 km	> 0.05 km
	Water Velocity, m/s	3 to 4 m/s*						
	References	Soria et al., 2016 *Ramos et al., 2014	Soria et al., 2016	Hori et al., 2007	Jankaew et al., 2008	Hawkes et al., 2007	Hawkes et al., 2007	Hawkes et al., 2007
Sedimentary textures and structures — Trench Scale	Thickness	2 cm (distal) 10–20 cm (proximal)	2 to 8 cm	> 20 to 33 cm (topographic lows), < 5 cm topographic highs	5 to 20 cm	15 cm	11 cm	30 cm
	Vertical grading of entire deposit	Unit 1 (sand sheet to mud): coarsening upward Unit 2 (washover terrace): coupled fining and coarsening upward	No analysis	Multiple normal grading	Overall upward fining	Multiple fining upward sequences separated by med to coarse sand layers	2 fining upward sequences	1 fining upward sequence
	Sorting	Moderate to well–sorted	Poorly sorted	Not reported	Poor to moderately sorted	Not reported	Not reported	Not reported
	Sedimentary structures	Unit 1: massive to horizontal planar lamination Unit 2: subhorizontal planar laminae	Massive	Thin, planar	Horizontal bedding			Shell fragments present, assymetrical current ripples
	Basal contact	Sharp, depositional	Sharp, depositional	Sharp, erosional	Sharp	Abrupt and erosional	Sharp and undulating	Sharp
Sedimentary textures and structures — Transect Scale	Cross–shore geometry	Washover terrace (proximal); sand sheet to mud (distal) with varying thickness landwards but generally thick in depressions	Overall but not systematic landward thinning			Little overwash sediments deposited on beach ridges but thicker deposits in swales	No transect data	No transect data	No transect data
	Lateral grading	Overall landward fining	Overall landward fining	No clear trend, coarser grained occur within 600 m from shoreline, finer sediments occur landward	Landward fining			
	Inland extent	1.6 km	350 m	1.1 km (bounded by scarps and hills)	> 1 km < 2km			
	References	This Study	This Study	Hori et al., 2007	Jankaew et al., 2008; Gouramanis et al., 2017	Hawkes et al., 2007	Hawkes et al., 2007	Hawkes et al., 2007

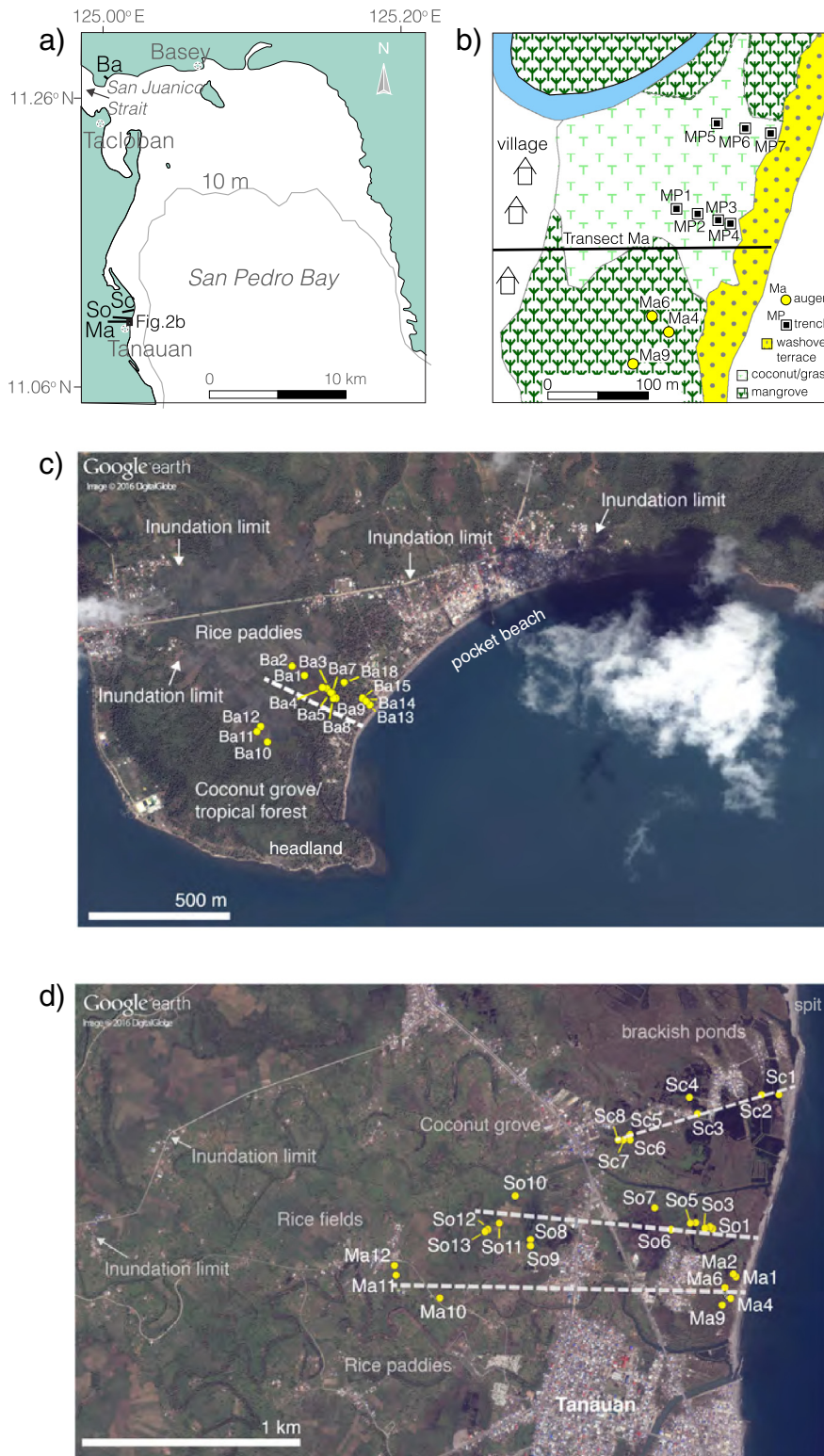* denotes corresponding reference.

Fig. 2. Study area and sampling location. (a) Index map of Basey and Tanauan transects and trenches. (b) Coastal environment and location of the trenches. (c) Basey transect Ba. (d) Tanauan transects Sc, So and Ma.

underlying pre-Haiyan soil that commonly contain buried upright grasses or root fragments. On the other hand, the contact between the Haiyan overwash sediments and the underlying agricultural soil in the rice paddies >400 m from the shore was gradational and started to be obscured by rapid post-typhoon vegetation growth (Fig. 3d).

The Haiyan overwash sediments on the siliciclastic coast of Tanauan display notable spatial variations, but not necessarily systematic trends (Fig. 5a–c). Along each of the transects (Sc, So, and Ma), the Haiyan sediments have variable thickness; the thickest accumulations of 5 to 7 cm were consistently found in topographic lows such as channels within the mangrove stands (*Nypa* forests) and depressions (shallow

a) Ba14

b) Ba3

c) Ma9

d) So12

Fig. 3. Sediment samples taken along transects in Basey and Tanauan. (a) Ba14 and (b) Ba3 in transect Ba. (c) Ma9 in transect Ma, (d) So12 in transect So.

ponds) between 200 and 400 m from the shore (Fig. 5a–c, ii). These thick Haiyan sediments are predominantly grey, moderately- to well-sorted (Fig. 5a–c, iv), fine (3ϕ) to coarse (1ϕ) sand (Fig. 5a–c, iii) that contain low amounts of organic matter (<10%; Fig. 5a–c, vi) and carbonate (<1%; Fig. 5a–c, vii). Between 500 m to ~1.6 km inland, rice paddies are blanketed by 1-cm to 3-cm thick accumulations of sediments with mean grain size ranging from silt (5ϕ) to very fine (4ϕ) sand (Fig. 5a–c, ii). A micro-topographic depression within the rice paddies resulted in an unusually thick (8 cm) Haiyan deposit at Ma10. Collectively, the Haiyan sand sheet within 400 m of the shore is distinctly coarser grained (1 to 3ϕ), better sorted (Fig. 5a–c, iv), and contains <10% organic matter. This is in contrast to the overwash sediments found >400 m from the shore (Fig. 5a–c, iii–iv).

Table 1 shows a comparative summary of the Haiyan overwash deposits observed at our transects as well as previous transects described by Abe et al. (2015) and Brill et al. (2016) in a nearby coastal area. Sedimentary features such as planar laminations, and multiple coarsening and fining sequences are common across all sites. However, the inland extent of the Haiyan deposit is clearly different. The Haiyan sandsheet at Tanauan and Tolosa reached >100 m (Abe et al., 2015) to ~250 m inland (Brill et al., 2016). We mapped the Haiyan overwash deposits and found that they extended farther inland, reaching 900 m (transect Sc) to as much as 1.6 km from the shore (transects So and Ma).

5.2.2. Trench-scale investigations

Trenches MP4 and MP7 revealed two different sedimentary units that overlie the pre-Haiyan soil surface. In trench MP4, Unit 1 is a ~10 cm thick accumulation of black, magnetite-rich, medium sand (1 to 2 ϕ) that coarsens upwards (Fig. 6). The sands of Unit 1 are

moderately sorted with sorting values remaining constant at ~0.75 ϕ (Fig. 6c). Thin planar laminations within the magnetite-rich Unit 1 sand were observed on the shore-perpendicular wall of trench MP7 (Fig. 7a). The planar laminations, however, appear wavy on the shore-parallel trench wall (Fig. 7b). The magnetite-rich sand of Unit 1 is overlain by the 12-cm thick, light grey, coarse sand (−1 to 0 ϕ) of Unit 2 (Figs. 6a–b, 7a–c). The contact between the two sediment units is very sharp and conformable, except on MP7, which has an erosional contact (Fig. 7b). The base of Unit 2 is characterized by relatively high concentrations of gravel-sized sediments displaying a fining upwards trend (Fig. 6c). At 5 cm from the surface, the initial fining upward sequence shifted to one that is coarsening upward to the surface. In contrast, the vertical grading in trench MP7 is not as complex as in trench MP4. Fig. 7d shows the bulk sediment mean grain size in MP7, which indicates a single and consistently coarsening upward sequence. Despite the coarsening upward trend in grain size, sorting remains uniform, and the entire sequence is composed of moderately sorted sediments (Figs. 6c, 7d). The laminated, magnetite-rich basal unit (Unit 1) did not persist beyond 50 m from the shore. Inland trenches MP6 and MP1 revealed thinner Haiyan deposits, which consist of a grey (10YR 5/1), medium sand (1.5 to 2 ϕ) that is relatively finer than Unit 1 and Unit 2 in the more seaward trenches MP4 and MP7 (Fig. 8).

6. Discussion

6.1. Textural and compositional variability of the Haiyan overwash deposit

The Haiyan overwash sediments close to the shores in Tanauan and in Basey exhibit notable differences in sediment composition, texture, and stratification. At Basey (Fig. 4), the Typhoon Haiyan sediments are
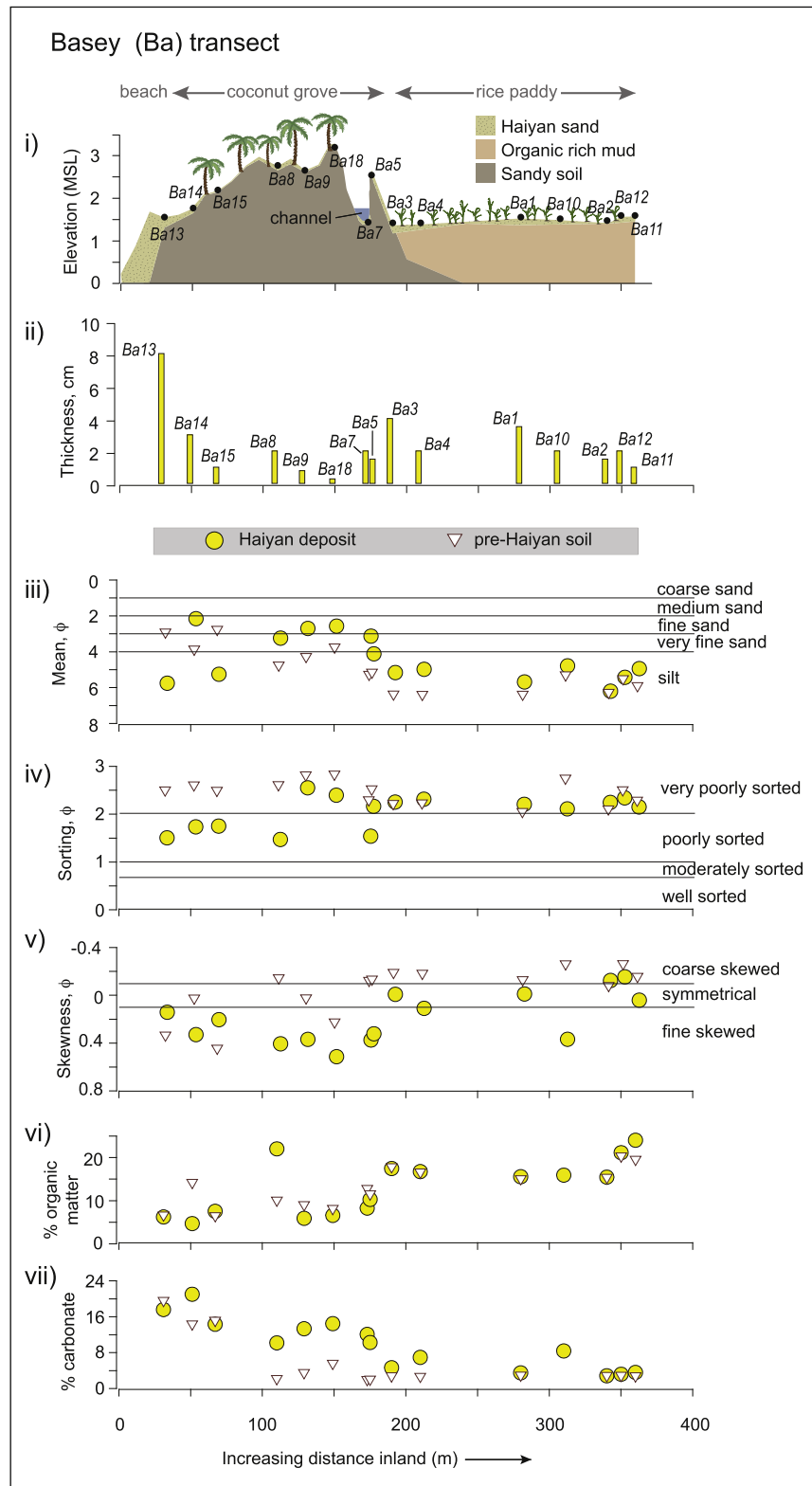
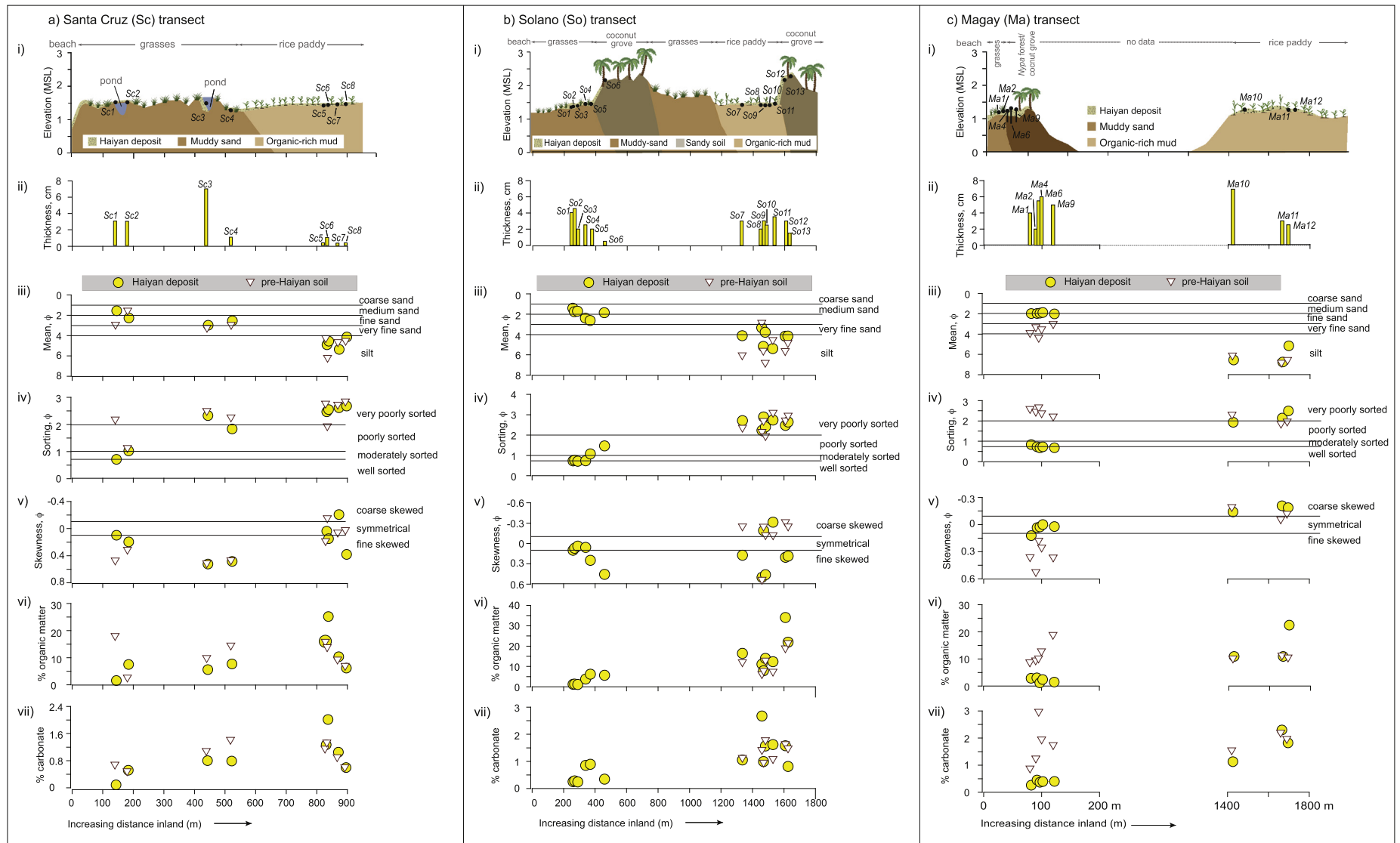**Fig. 4.** Sediment data along transect Ba. (i) Across-shore profile and sample locations, (ii) thickness of Haiyan deposits, (iii) mean grain size, (iv) sorting, (v) skewness, (vi) organic matter content, (vii) carbonate content.

generally characterized by a massive, poorly sorted, fine sand that contains carbonate material ranging from 5 to 24%, including foraminifera, and fragments of mollusks and corals (Pilarczyk et al., 2016). In contrast, the Typhoon Haiyan sediments from Tanauan (Fig. 5) are moderately to well-sorted, medium to coarse sand containing very low carbonate

concentrations of <3%. Heavy minerals are relatively abundant and accumulate in layers (Figs. 6a, 7a–b). Thin planar laminations were also visible within the deposit (Fig. 7a, b).

The significant disparity in the carbonate content between the Haiyan overwash sediments from Basey and Tanauan is indicative of

Fig. 5. Sediment data along transects (a) Sc, (b) So and (c) Ma. (i) Across-shore profile and sample locations, (ii) thickness of Haiyan deposits, (iii) mean grain size, (iv) sorting, (v) skewness, (vi) organic matter content, (vii) carbonate content.

a)

b)

c)
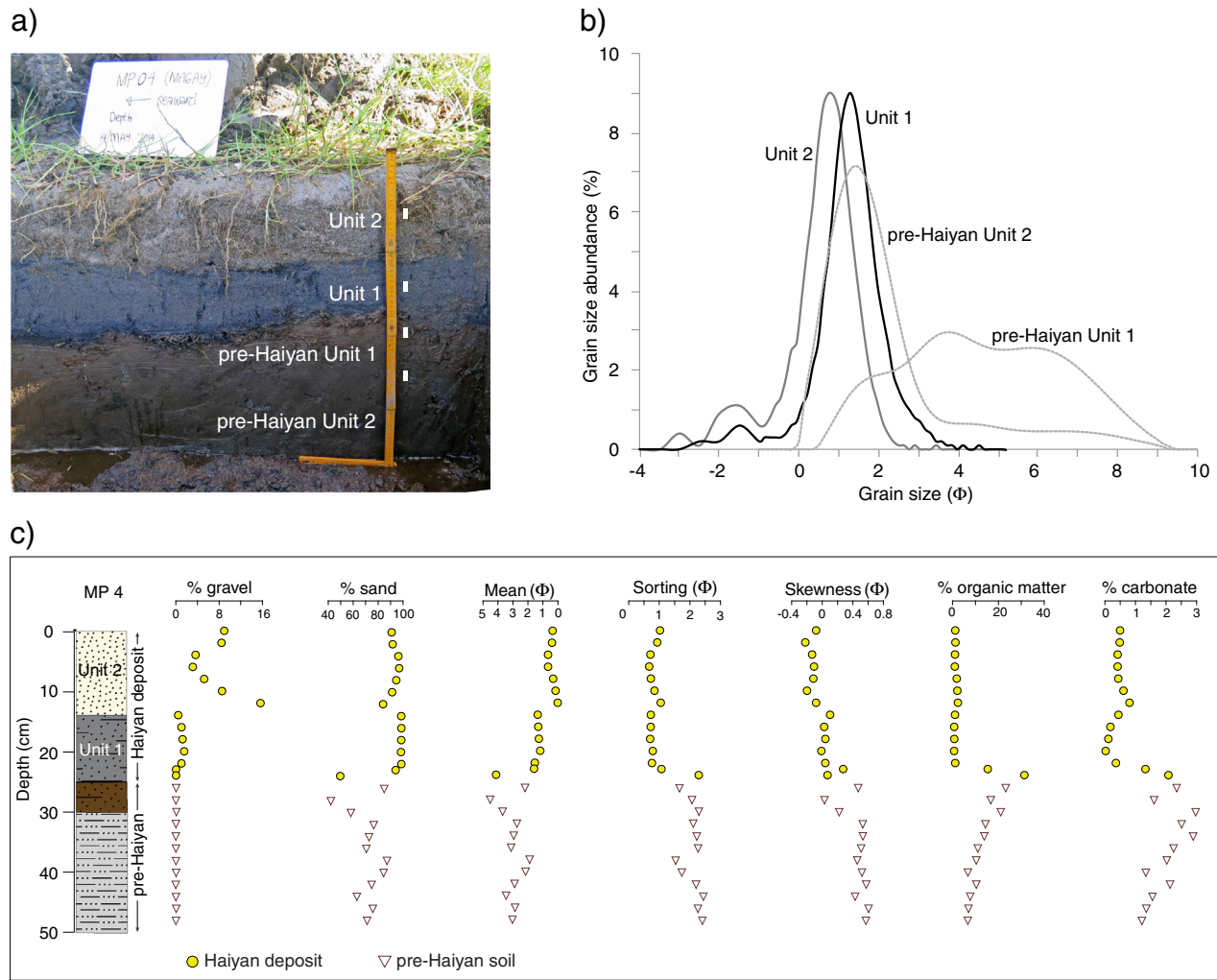
Fig. 6. Trench MP4. (a) Trench wall perpendicular to the shore. (b) Grain size distribution of each sediment unit. (c) Stratigraphic relationship and contrasting sedimentological characteristics between the Haiyan deposit and the underlying pre-Haiyan soil.

the sediment source. Carbonate sediments are naturally readily available in the mixed carbonate-siliciclastic coast of Basey, but rare in the non-carbonate, siliciclastic coast of Tanauan (Aurelio and Peña, 2002; Suerte et al., 2005). Similarly, Pilarczyk et al. (2016) reported two distinct foraminiferal assemblages corresponding to the two contrasting environments. The overwash sediments on the mixed carbonate-siliciclastic coast contained significantly higher concentrations of calcareous foraminifera (45–6320 foraminifera per 5 cm³) compared to the overwash sediments on the siliciclastic coast of Tanauan that contained only 5–80 foraminifera per 5 cm³.

At both sites, however, the most inland Haiyan overwash sediments share commonalities in grain size, texture, and composition (Figs. 4,5). The sediments are very poorly sorted, ranging from silt to very fine sand, and contain a higher amount of organic matter ranging from 10 to 35%, and lower concentrations of carbonate at <5%. The Haiyan overwash sediments occur as anomalous sand layers over muddy sediments up to distances of 200 m (Basey, Fig. 4, ii) to 400 m (Tanauan, Fig. 5a–c, ii) from the shore, which is less than the inundation limit. Beyond 200 m (Basey, Fig. 4, ii) to 400 m (Tanauan, Fig. 5a–c, ii), granulometry does not reliably discriminate the overwash sediments from the pre-storm sedimentary layers. As such, the textural definition of overwash sediments as "anomalous sand layers" may not necessarily be the most appropriate term, particularly for sediments deposited closest to the inundation limit. The distal deposit of Typhoon Haiyan is

mud-dominated and similar to the Hurricane Rita deposit (Williams, 2009). In addition, the distinct textural and compositional signatures associated with the Typhoon Haiyan deposit closest to the shore seemed to be less evident inland. The notable sedimentologic differences associated with landward distance are consistent with the established distance-related micropaleontologic clustering reported by Pilarczyk et al. (2016). Concentrations of testate amoebae and small foraminifera were higher in more inland overwash sediments in Basey (>160 m) and in Tanauan (>400 m) compared to the overwash sediments found near the shore (Pilarczyk et al., 2016).

6.2. Spatial variability in the sedimentation pattern of the Haiyan overwash deposit

Another notable difference between the overwash sediments in Tanauan and in Basey is the inland extent. The overwash sediments along transects Sc, So, and Ma in Tanauan reached greater distances inland than the overwash sediments along transect Ba in Basey (Figs. 4, 5). The inland extent of overwash sediments is likely to be related to the inundation distance at each site, which is mainly controlled by topographic relief. The low (1 to 2 m), gently sloping terrain in Tanauan promoted greater inundation distance to ~2 km, but the overwash sediments reached a landward extent of only ~1.6 km (Fig. 5a–c, i–ii). The relatively irregular topography of raised carbonate platforms (3 m)
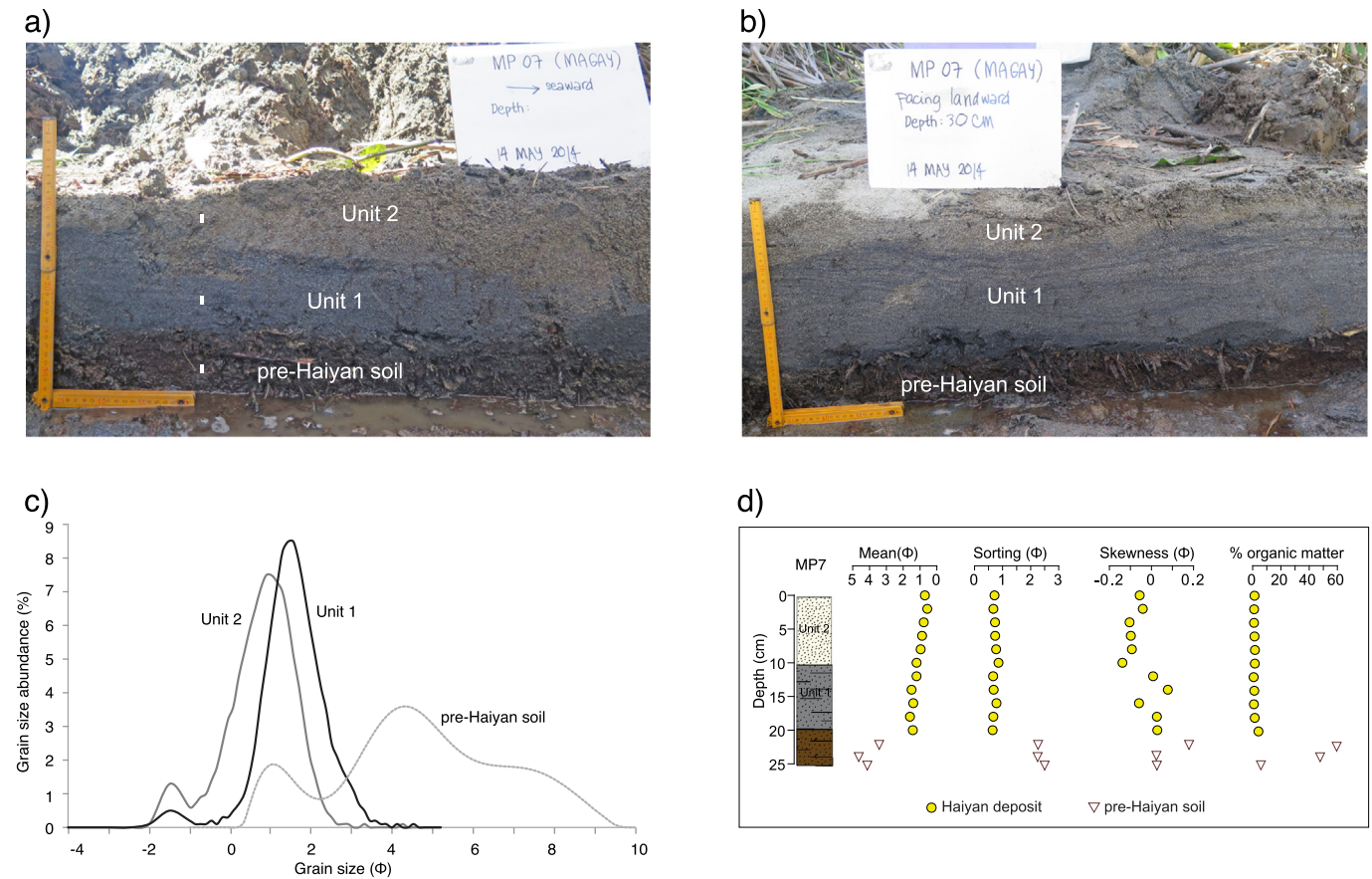
Fig. 7. Trench MP7. (a) Trench wall perpendicular to the shore. (b) Trench wall parallel to the shore. (c) Grain size distribution of each sediment unit. (d) Stratigraphic relationship and contrasting sedimentological characteristics between the Haiyan deposit and the underlying pre-Haiyan soil.

and rice paddies on terraced slopes in Basey limited inland inundation to ~800 m, with overwash sedimentation reaching to ~350 m inland (Fig. 4, i–ii). We argue that given similar surge levels at both sites, the local topography exerts significant control on overland inundation distance and therefore the inland extent of the deposits. Similarly, the differences in the extent and thickness of overwash deposits from Hurricane Ike were attributed to site-specific geomorphology and surge/wave conditions (Williams, 2010; Hawkes and Horton, 2012) (Table 2). The topography-dependent inland extent was also observed in the 2004 tsunami deposit across the affected coasts surrounding the Indian Ocean. The 2004 Indian Ocean tsunami deposit reached a greater inland extent (up to 2 km) along broad, low relief beach-ridge coasts in Thailand (Hori et al., 2007; Jankaew et al., 2008) than the inland extent (350 to 400 m) in narrow, steep beaches in Thailand, Indonesia, India, and Sri Lanka (e.g., Moore et al., 2006; Hawkes et al., 2007; Srinivasalu et al., 2007; Morton et al., 2008; Switzer et al., 2012).

Even within similar coastal environments, topographic relief, overland flow depth, and inundation extent, the inland extent of the Haiyan deposit differs distinctly between Tanauan and Tolosa (Table 1). Contrary to earlier reports of overwash sedimentation from Typhoon Haiyan extending <300 m (e.g., Abe et al., 2015; Brill et al., 2016; Watanabe et al., 2017), we documented greater inland extents of 900 m to ~1.6 km. This suggests that other local conditions beyond the scope of this study may likely contribute to the spatial variations, including vegetation (e.g., Gelfenbaum et al., 2007; Wang and Horwitz, 2007; Watanabe et al., 2017) or the interaction of multiple waves (e.g., Apotsos et al., 2011). The coastal vegetation cover in Tanauan and Tolosa varies from coconut grove, mangrove stands (*Nypa* forest), and grasses (including rice). Small-scale topographic changes in each vegetation zone appear to create localized depositional sites (e.g., Hori

et al., 2007; Apotsos et al., 2011). For example, small channels within the *Nypa* forest or micro-topographic depressions in the rice paddies (e.g., Ma 10) allowed for thicker accumulations of the Haiyan deposit relative to surrounding areas. Vegetation also affects sedimentation patterns by changing the overland flow conditions. Each vegetation type has a different height and density that results in varying bed shear stress, which in turn can modify overland flow conditions that will lead to variability in the inland extent and thicknesses of overwash deposits (Watanabe et al., 2017). More detailed sediment transport modeling on sediments from the Tanauan transects (Sc, So, Ma, and trenches MP1–7) may provide insights into the relative contributions of these local factors (e.g., Gelfenbaum et al., 2007; Tang and Weiss, 2015).

6.3. Sedimentologic indicators of storm surge flow and depositional regimes

The two sub-units (Unit 1 and Unit 2) of the Haiyan deposit in Tanauan (Figs. 6, 7) can be attributed to either different inundation regimes (e.g., Williams, 2009; Hawkes and Horton, 2012) or multiple wave arrivals (e.g., Leatherman and Williams, 1977; Sedgwick and Davis, 2003; Switzer and Jones, 2008). Eyewitness accounts and storm surge modeling confirm three wave sets within the duration of Haiyan's storm surge inundation (Soria et al., 2016). Unit 1 and Unit 2 are separated by a sharp, depositional to erosional contact, which suggests that each unit resulted from different flow regimes. It is possible that Unit 1 and Unit 2 resulted from the multiple wave sets during Haiyan inundation, but we cannot attribute an individual unit to a single wave set. There seems to be no one-to-one correspondence between the number of waves and the number of sub-units or layers within an event deposit (e.g., Gelfenbaum and Jaffe, 2003; Hawkes et al., 2007).
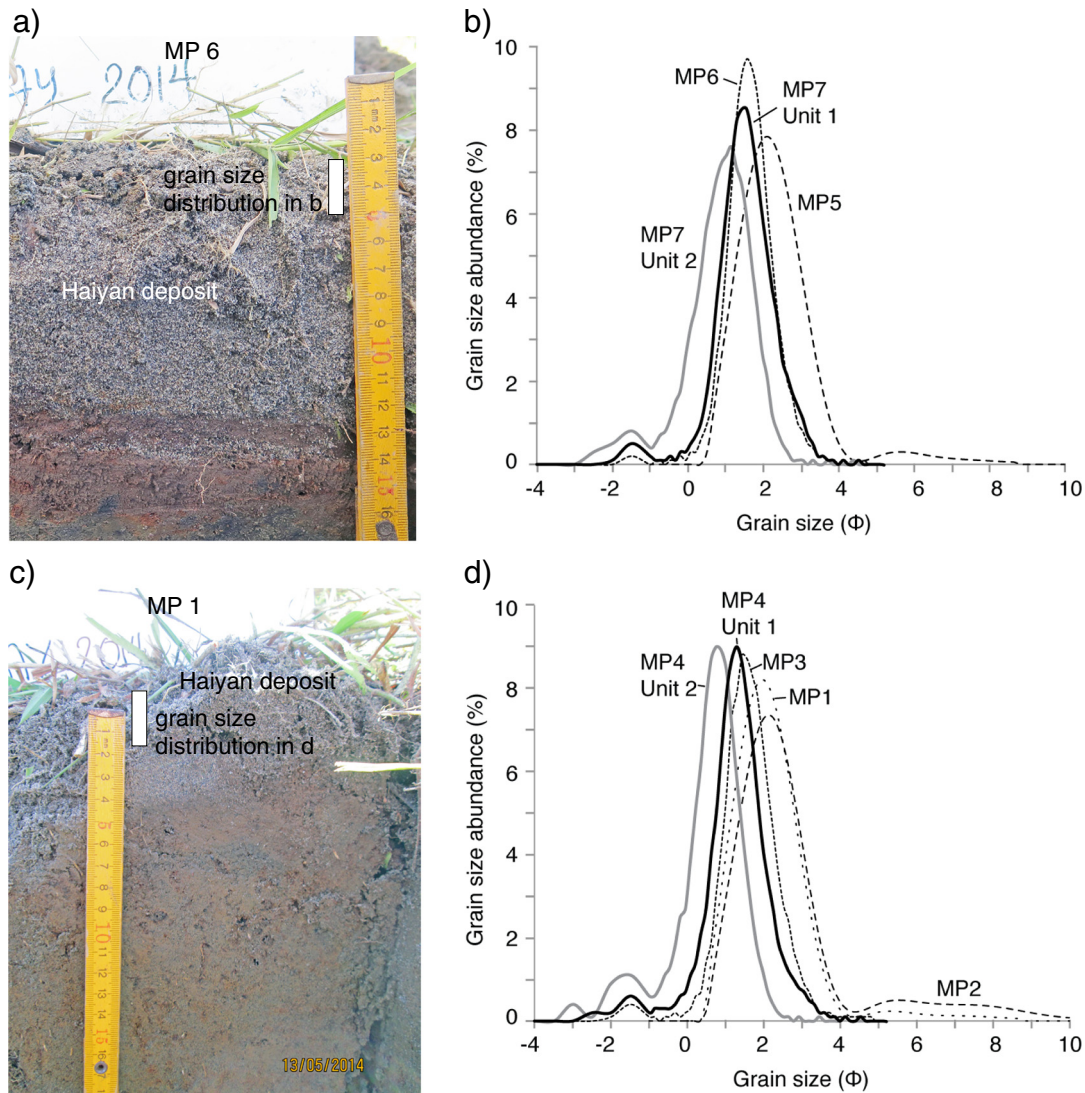
Fig. 8. Typhoon Haiyan overwash sand revealed on the inland trenches. (a) ~8 cm thick Haiyan sand in trench MP6. (b) Grain size distribution of Haiyan sand along transect MP5 to MP7. (c) ~4 cm thick Haiyan sand in trench MP1. (d) Grain size distribution of Haiyan sand along transect MP1 to MP 4.

Alternatively, Unit 1 and Unit 2 of the Haiyan deposit may represent different depositional phases corresponding to varying inundation regimes similar to that observed during Hurricane Rita (Williams, 2009). The laminated, coarsening upward, magnetite-rich basal sand in Unit 1 was most likely deposited by suspension associated with the deep flow and bore-type flooding of Typhoon Haiyan (e.g., Wang and Horwitz, 2007; Williams, 2009). In contrast, the coarser, massive sand characterized by Unit 2 is likely to have been deposited as a traction load of the washover terrace (e.g., Williams, 2009; Brill et al., 2016), either at the latter stage of Haiyan flooding or from smaller overwash from the first phase of recovery immediately following the typhoon. In addition, the coarsening upward trend in both sand units (Figs. 6c, 7d) may be due to increasing surge velocity either upon the arrival of the first waves or during backflow. This is similar to other intense hurricanes such as Hurricanes Rita and Ike (Horton et al., 2009; Hawkes and Horton, 2012).

Overall, the two sub-units within the Haiyan overwash deposit display planar laminations and coarsening upward trends (Figs. 6c, 7d), jointly indicating upper flow regime conditions of a unidirectional, turbulent, high velocity flow (Cheel, 1990; Fielding, 2006), which is consistent with the bore-type storm surge of Typhoon Haiyan (Soria et al., 2016). In-situ field measurements of storm overwash with a 0.7 m-deep surge in

Assateague Island on the U.S. Atlantic coast during Category 1 hurricanes yielded overwash flow velocities about 2 to 3.5 m s^{-1} (Leatherman, 1976; Fisher and Stauble, 1978). Comparably, a 1-m deep Typhoon Haiyan flood on the coast 15 km to the south of Tanauan had estimated flow velocities that ranged between 3 and 4 m s^{-1} (Ramos et al., 2014). A deeper surge flood of at least 3 m in Tacloban yielded velocities as high as 7 m s^{-1}, but these elevated velocities were mainly due to channelized flows on the streets in an urban setting (Takagi et al., 2016). These flow velocities are relatively stronger than the previously modelled overland flow velocity of Haiyan's surge in Tacloban not exceeding 2 m s^{-1} (Bricker et al., 2014) and within the lower range of a tsunami flow such as the 2011 Tohoku tsunami (Hayashi and Koshimura, 2012). Our extensive sediment data can be used in sediment transport modeling to substantiate sparse overland flow velocity estimates.

6.4. Haiyan and other modern storm and tsunami overwash events

Typhoon Haiyan's bore-like storm surge appears uncommon among the recent notable storm surges worldwide (Mikami et al., 2016). Table 2 shows that Typhoon Haiyan's storm surge had exceptionally short flooding duration resulting in a steep storm surge profile (Soria et al., 2016) compared to similarly intense modern storms (Fritz et al.,

2007; Doran et al., 2009; Boughton et al., 2011; Morton and Barras, 2011; McGee et al., 2013; Takagi et al., 2015). It is not surprising then that flow velocities associated with the Haiyan surge were as high as 3 to 4 m s^{-1} (Ramos et al., 2014) to 7 m s^{-1} (Takagi et al., 2016), which are within the range of the flow velocities of the 2011 Tohoku tsunami on a similar gently sloping coast of Sendai Plain (Abe et al., 2012; Sugawara and Goto, 2012; Hayashi and Koshimura, 2012) (Table 3). Perhaps this apparent similarity of Haiyan's storm surge to tsunami flooding has influenced overwash sedimentation such that although there are apparent differences, the sedimentary features are for the most part equivocal of either storm or tsunami deposits.

The Typhoon Haiyan overwash deposit displays similar sedimentary structures and stratigraphic relationships as those from comparably intense storms, but shows different patterns of sediment thickness and landward extent (Table 2). Modern overwash deposits commonly display a landward fining trend, planar laminae, and sharp basal contact with the underlying pre-storm sequence, although the nature of the contact can be either depositional or erosional (e.g., Morton et al., 2007; Horton et al., 2009; Williams, 2009, 2010; Hawkes and Horton, 2012; Nott et al., 2013). Deposit thickness is often variable. The overwash deposits resulting from Typhoon Haiyan and Hurricane Katrina are notably thin (<20 cm) compared to Cyclone Yasi, and Hurricanes Ike, Rita, Isabel, and Carla (40 cm to <1 m). The thicker storm deposits are typically associated with the washover terraces or fans that are formed at a limited extent from the shore (e.g. Morton et al., 2007; Williams, 2009; Nott et al., 2013). Many of the overwash deposits from recent storms show landward extents that are limited to <100 m. For example, sediments deposited by Cyclone Yasi reached a distance of ~80 m only (Nott et al., 2013). This is in contrast to Typhoon Haiyan, and Hurricanes Ike and Carla, which deposited sediments up to ≥1 km inland (Morton et al., 2007; Williams, 2010) (Table 2).

The Typhoon Haiyan overwash deposit exhibits sedimentary structures that are also observed in recent tsunami deposits. The Typhoon Haiyan overwash deposit displays both fining and coarsening upward trends, but not systematic landward fining. The deposit was also found to be massive or exhibit planar laminae. These sedimentary features have also been associated with tsunami deposits (Table 3), including those resulting from the 2011 Tohoku-oki (Abe et al., 2012; Takashimizu et al., 2012), 2006 Western Java (Moore et al., 2011), and 2004 Indian Ocean earthquakes and tsunamis (e.g., Moore et al., 2006; Hawkes et al., 2007; Morton et al., 2008; Switzer et al., 2012) (Tables 4,5). In addition, the Haiyan deposit is comparably thin (<30 cm), which is similar to the recent tsunami deposits of the 2011 Tohoku, 2006 West Java, and 2004 Indian Ocean tsunamis (Tables 3–5). However, thicker tsunami deposits, reaching maximum thicknesses of 40 cm, have also been reported for the 2011 Tohoku tsunami (Abe et al., 2012) and 2004 Indian Ocean tsunami (Srinivasalu et al., 2007; Switzer et al., 2012).

The maximum inland extent of the Haiyan deposit shows notable similarities and differences with recent tsunami deposits (Tables 3-5). For example, given similar topography and overland flow conditions, the inland extent of the Typhoon Haiyan deposit at Basey is comparable to the 2004 Indian Ocean tsunami deposits on the narrow, steep beaches in Indonesia, India, and Sri Lanka. The overwash deposits typically reached distances between 350 m and 400 m inland (Moore et al., 2006; Srinivasalu et al., 2007; Morton et al., 2008; Switzer et al., 2012) (Table 4). In the same way, the inland extent of the Typhoon Haiyan deposit at Tanauan is comparable with the 2004 Indian Ocean tsunami deposit along broad beach-ridge coasts in Thailand. The overwash deposits reached distances ranging from >1 km but not exceeding 2 km inland (Hori et al., 2007; Jankaew et al., 2008) (Table 5). Although the coastal setting and overland flow depth are comparable, the Typhoon Haiyan overwash deposit has limited maximum inland extent of <2 km compared to that of the 2011 Tohoku tsunami reaching to 4 km (Abe et al., 2012; Takashimizu et al., 2012) (Table 3).

The stark contrast between the Typhoon Haiyan overwash deposit in Leyte Gulf and recent tsunami deposits can be seen in the nature of the basal contact. The recent tsunami deposits typically exhibit an erosional base (Tables 3–5), whereas the Typhoon Haiyan deposit exhibits a depositional base in most instances, but rarely erosional (Table 1).

This comparative study of the Typhoon Haiyan deposit with other recent storm and tsunami deposits elsewhere illustrates that the inland extent and thickness of overwash sedimentation are widely variable, and there is no distinctive pattern between storm and tsunami deposits (Tables 2–5). The inland extent and thickness of overwash sedimentation are seemingly due to dynamic interaction of several site-specific factors including topographic relief, inundation limit, and overland flow conditions (e.g., Morton et al., 2007; Hawkes and Horton, 2012; Apotsos et al., 2011). Contrary to the numerical modeling results of Watanabe et al. (2017), empirical data of modern overwash sediments show that the maximum inland extent and thickness of sedimentation, by virtue of the local variability, may not necessarily provide conclusive evidence for distinguishing between storm and tsunami deposits.

7. Conclusions

Typhoon Haiyan deposits present clear evidence that the interaction between local geology, coastal topographic relief and hydrodynamic conditions strongly influence inland sedimentation during storm inundation. Despite the similar storm surge levels between Tanauan and Basey, Typhoon Haiyan left starkly contrasting sediments at both locations, underscoring the effect of local geology and topographic relief. On the mixed siliciclastic-carbonate coast of Basey, the Haiyan overwash sediments are carbonate-rich, poorly-sorted, silt to fine sand. In contrast, on the siliciclastic coast of Tanauan, the Haiyan overwash sediments are carbonate-poor, predominantly grey, moderately- to well-sorted, fine to coarse sand. Moreover, the low-lying flat terrain in Tanauan promoted greater inland penetration of the surge (2 km) and therefore of the overwash deposit (~1.6 km), whereas the relatively irregular topography associated with raised carbonate platforms and rice paddies on terraced slopes in Basey limited landward overwash sedimentation (~400 m). The thickest deposits (8 to 20 cm) were observed locally in topographic lows such as in shallow depressions and ponds. Notably, the inland extent of the Haiyan deposit varied spatially at places such as Tanauan and Tolosa, even though the depositional setting, topographic relief, overland flow depth, and inundation extent were similar. We infer that spatial variations in thickness and inland extent of the Typhoon Haiyan deposit may be additionally attributed to the different type of vegetation cover.

On a global scale, the Typhoon Haiyan deposit represents a sediment record of an extreme storm surge that exhibited flooding characteristics not typical of storm inundation. The short flooding duration with elevated flow depths and flow velocities are rare characteristics among recent notable storm surges worldwide and are more comparable to tsunami flooding. The Haiyan deposit exhibits planar stratification, a coarsening upward sequence, an overall but non-systematic landward fining trend, and a sharp depositional (rarely erosional) basal contact with the underlying substrate. Given similar topographic relief and overland flow conditions, Typhoon Haiyan deposits show comparable sedimentation patterns in terms of the thickness (<30 cm) and landward extent (hundred of meters up to 2 km) with the 2004 Indian Ocean tsunami deposits. Overall, the Haiyan deposits have sedimentologic and stratigraphic characteristics that show a hybrid signature common to both storm and tsunami deposits.

Appendix A. Supplementary data

Supplementary data to this article can be found online at http://dx.doi.org/10.1016/j.sedgeo.2017.06.006.

References

Abe, T., Goto, K., Sugawara, D., 2012. Relationship between the maximum extent of tsunami sand and the inundation limit of the 2011 Tohoku-oki tsunami on the Sendai Plain. Sedimentary Geology 282, 142–150.

Abe, T., Goto, K., Sugawara, D., Suppasri, A., 2015. Geological traces of the 2013 Typhoon Haiyan in the Southeast coast of Leyte Island. Second Report of IRIDeS Fact-Finding Mission to Philippines. Tohoku University International Research Institute of Disaster Science, pp. 169–174.

Apotsos, A., Gelfenbaum, G., Jaffe, B., 2011. Process-based modeling of tsunami inundation and sediment transport. Journal of Geophysical Research 116, F01006. http://dx.doi.org/10.1029/2010JF001797.

Aurelio, M.A., Peña, R.E., 2002. Geology and Mineral Resources of the Philippines. vol. 1. Department of Environment and Natural Resources Mines and Geosciences Bureau, Philippines, pp. 277–300.

Blott, S.J., Pye, K., 2001. GRADISTAT: a grain size distribution and statistics package for the analysis of unconsolidated sediments. Earth Surface Processes and Landforms 26, 1237–1248 (GRADISTAT Program. Downloaded at http://www.kpal.co.uk/gradistat.html).

Boughton, G.N., Henderson, D.J., Ginger, J.D., Holmes, J.D., Walker, G.R., Leitch, C.J., Somerville, L.R., Frye, U., Jayasinghe, N.C., Kim, P.Y., 2011. Tropical Cyclone Yasi: structural damage to buildings. Technical Report No. 57. James Cook University, pp. 1–15.

Bricker, J., Takagi, H., Mas, E., Kure, S., Adriano, B., Yi, C., Roeber, V., 2014. Spatial variation of damage due to storm surge and waves during Typhoon Haiyan in the Philippines. Journal of Japan Society of Civil Engineers, Series B2 (Coastal Engineering) 70, I_231–I_235.

Brill, D., May, S.M., Engel, M., Reyes, M., Pint, A., Opitz, S., Dierick, M., Gonzalo, L.A., Esser, S., Brückner, H., 2016. Typhoon Haiyan's sedimentary record in coastal environments of the Philippines and its palaeotempestological implications. Natural Hazards and Earth System Sciences 16, 2799–2822.

Buynevich, I.V., FitzGerald, D.M., Van Heteren, S., 2004. Sedimentary records of intense storms in Holocene barrier sequences, Maine, USA. Marine Geology 210, 135–148.

Cheel, R.J., 1990. Horizontal lamination and the sequence of bed phases and stratification under upper-flow-regime conditions. Sedimentology 37, 517–529.

Dean, W.E., 1974. Determination of carbonate and organic matter in calcareous sediments and sedimentary rocks by loss on ignition: comparison with other methods. Journal of Sedimentary Petrology 44, 242–248.

Donnelly, J.P., Butler, J., Roll, S., Wengren, M., Webb III, T., 2004. A backbarrier overwash record of intense storms from Brigantine, New Jersey. Marine Geology 210, 107–121.

Doran, K.S., Plant, N.G., Stockdon, H.F., Sallenger, A.H., Serafin, K.A., 2009. Hurricane Ike: Observations of Coastal Change: U.S. Geological Survey Open-File Report, 2009-1061. p. 35.

Fielding, C.R., 2006. Upper flow regime sheets, lenses and scour fills: extending the range of architectural elements for fluvial sediment bodies. Sedimentary Geology 190, 227–240.

Fisher, J.S., Stauble, D.K., 1978. Washover and dune interaction on a barrier island. Proceedings Coastal Zone '78. ASCEi, San Francisco, California, pp. 1611–1618.

Flater, D., 1998. XTide: harmonic tide clock and tide predictor accessed on 25 May 2014. www.flaterco.com/xtide/.

Folk, R.L., Ward, W.C., 1957. Brazos River bar: a study in the significance of grain size parameters. Journal of Sedimentary Petrology 27, 3–26.

Fritz, H.M., Blount, C., Sokoloski, R., Singleton, J., Fuggle, A., McAdoo, B.G., Moore, A., Grass, C., Tate, B., 2007. Hurricane Katrina Storm surge distribution and field observations on the Mississippi barrier islands. Estuarine, Coastal and Shelf Science 74, 12–20.

Fritz, H.M., Phillips, D.A., Okayasu, A., Shimozono, T., Liu, H., Mohammed, F., Skanavis, V., Synolakis, C.E., Takahashi, T., 2012. The 2011 Japan tsunami current velocity measure-

ments from survivor videos at Kesennuma Bay using LiDAR. Geophysical Research Letters 39, L00G23. http://dx.doi.org/10.1029/2011GL050686.

Gelfenbaum, G., Jaffe, B., 2003. Erosion and sedimentation from the 17 July, 1998 Papua New Guinea tsunami. Pure and Applied Geophysics 160, 1969–1999.

Gelfenbaum, G., Vatvani, D., Jaffe, B., Dekker, F., 2007. Tsunami inundation and sediment transport in the vicinity of coastal mangrove forest. In: Kraus, N.C., Rosati, J.D. (Eds.), Coastal Sediments '07. American Society of Civil Engineers, Reston, Va, pp. 1117–1129.

Goff, J., McFadgen, B.G., Chagué-Goff, C., 2004. Sedimentary differences between the 2002 Easter storm and the 15th-century Okoropunga tsunami, southeastern North Island, New Zealand. Marine Geology 204, 235–250.

Goto, K., Okada, K., Imamura, F., 2009. Characteristics and hydrodynamics of boulders transported by storm waves at Kudaka Island, Japan. Marine Geology 262, 14–24.

Gouramanis, C., Switzer, A.D., Jankaew, K., Bristow, C.S., Pham, D.T., Ildefonso, S.R., 2017. High-frequency coastal overwash deposits from Phra Thong Island, Thailand. Scientific Reports 7:43742. http://dx.doi.org/10.1038/srep43742.

Hawkes, A.D., Horton, B.P., 2012. Sedimentary record of storm deposits from Hurricane Ike, Galveston and San Luis Islands, Texas. Geomorphology 171–172, 180–189.

Hawkes, A.D., Bird, M., Cowie, S., Grundy-Warr, C., Horton, B., Tan Shau Hwai, A., Law, L., Macgregor, C., Nott, J., Eong Ong, J., Rigg, J., Robinson, R., Tan-Mullins, M., Tiong Sa, T., Zulfigar, Y., 2007. The sediments deposited by the 2004 Indian Ocean Tsunami along the Malaysia–Thailand Peninsula. Marine Geology 242, 169–190.

Hayashi, S., Koshimura, S., 2012. Measurement of the 2011 Tohoku tsunami flow velocity by the aerial video analysis. Journal of Japan Society of Civil Engineers, Series B2 (Coastal Engineering) 68, 366–370.

Heiri, O., Lotter, A.F., Lemcke, G., 2001. Loss on ignition as a method for estimating organic and carbonate content in sediments: reproducibility and comparability. Journal of Paleolimnology 25, 101–110.

Hori, K., Kuzumoto, R., Hirouchi, D., Umitsu, M., Janjirawuttikul, N., Patanakanog, B., 2007. Horizontal and vertical variation of 2004 Indian tsunami deposits: an example of two transects along the western coast of Thailand. Marine Geology 239, 163–172.

Horton, B.P., Rossi, V., Hawkes, A.D., 2009. The sedimentary record of the 2005 hurricane season from Mississippi and Alabama coastlines. Quaternary International 195, 15–30.

Jankaew, K., Atwater, B.F., Sawai, Y., Choowong, M., Charoentitirat, T., Martin, M.E., Prendergast, A., 2008. Medieval forewarning of the 2004 Indian Ocean tsunami in Thailand. Nature 455, 1228–1231.

Kortekaas, S., 2002. Tsunamis, Storms and Earthquakes: Distinguishing Coastal Flooding Events. (Unpublished Ph.D. thesis). University of Coventry (179 pp).

Kortekaas, S., Dawson, A.G., 2007. Distinguishing tsunami and storm deposits: an example from Martinhal, SW Portugal. Sedimentary Geology 200, 208–221.

Leatherman, S.P., 1976. Assateague Island: a case study of barrier island dynamics. In: Leatherman, S.P. (Ed.), Overwash Processes. Benchmark Papers in Geology Vol. 58. Hutchinson Ross Publishing Company, Stroudsburg, PA, pp. 350–364.

Leatherman, S.P., 1981. Overwash processes. Benchmark Papers in Geology Vol. 58. Hutchinson Ross Publishing Co., USA (376 pp).

Leatherman, S.P., Williams, A.T., 1977. Lateral textural grading in overwash sediments. Earth Surface Processes 2, 333–341.

Lin, I.-I., Pun, I.-F., Lien, C.-C., 2014. "Category-6" supertyphoon Haiyan in global warming hiatus: contribution from subsurface ocean warming. Geophysical Research Letters 41, 8547–8553.

Liu, K.-b., Fearn, M.L., 1993. Lake-sediment record of late Holocene hurricane activities from coastal Alabama. Geology 21, 793–796.

Mas, E., Bricker, J., Kure, S., Adriano, B., Yi, C., Suppasri, A., Koshimura, S., 2015. Field survey report and satellite image interpretation of the 2013 Super Typhoon Haiyan in the Philippines. Natural Hazards and Earth System Sciences 15, 805–816.

McGee, B.D., Goree, B.B., Tollett, R.W., Woodward, B.K., Kress, W.H., 2013. Hurricane Rita surge data, Southwestern Louisiana and Southeastern Texas, September to November 2005. LC11. U.S. Geological Survey (http://pubs.usgs.gov/ds/2006/220/index.htm#elevsurveys accessed on 6 May 2016).

Mikami, T., Shibayama, T., Takagi, H., Matsumaru, R., Esteban, M., Thao, N.D., De Leon, M., Valenzuela, V.P., Oyama, T., Nakamura, R., Kumagai, K., Li, S., 2016. Storm surge heights and damage caused by the 2013 Typhoon Haiyan along the Leyte Gulf coast. Coastal Engineering Journal 58:1640005. http://dx.doi.org/10.1142/S0578563416400052.

Moore, A., Nishimura, Y., Gelfenbaum, G., Kamataki, T., Triyono, R., 2006. Sedimentary deposits of the 26 December 2004 tsunami on the northwest coast of Aceh, Indonesia. Earth, Planets and Space 58, 253–258.

Moore, A., Goff, J., McAdoo, B.G., Fritz, H.M., Guzman, A., Kalligeris, N., Kalsum, K., Susanto, A., Suteja, D., Synolakis, C.E., 2011. Sedimentary deposits from the 17 July 2006 Western Java Tsunami, Indonesia: use of grain size analyses to assess tsunami flow depth, speed, and traction carpet characteristics. Pure and Applied Geophysics 168, 1951–1961.

Morgerman, J., 2014. Super Typhoon Haiyan in Tacloban City and Leyte, Philippines. Accessed online on 4 February 2017. http://www.icyclone.com/upload/chases/haiyan/iCyclone_HAIYAN_in_Tacloban_City_040314.pdf.

Morton, R.A., Barras, J.A., 2011. Hurricane impacts on coastal wetlands: a half-century record of storm generated features from southern Louisiana. Journal of Coastal Research 27, 27–43.

Morton, R.A., Sallenger, A.H., 2003. Morphological impacts of extreme storms on sandy beaches and barriers. Journal of Coastal Research 19, 560–573.

Morton, R.A., Gelfenbaum, G., Jaffe, B.E., 2007. Physical criteria for distinguishing sandy tsunami and storm deposits using modern examples. Sedimentary Geology 200, 184–207.

Morton, R.A., Goff, J.R., Nichol, S.L., 2008. Hydrodynamic implications of textural trends in sand deposits of the 2004 tsunami in Sri Lanka. Sedimentary Geology 207, 56–64.

Nanayama, F., Shigeno, K., Satake, K., Shimokawa, K., Koitabashi, S., Mayasaka, S., Ishii, M., 2000. Sedimentary differences between 1993 Hokkaido-nansei-oki tsunami and 1959 Miyakojima typhoon at Tasai, southwestern Hokkaido, northern Japan. Sedimentary Geology 135, 255–264.

Nott, J., Chague-Goff, C., Goff, J., Sloss, C., Riggs, N., 2013. Anatomy of sand beach ridges: evidence from severe tropical cyclone Yasi and its predecessors, northeast Queensland, Australia. Journal of Geophysical Research: Earth Surface 118, 1710–1719.

Otvos, E.G., 2011. Hurricane signatures and landforms—toward improved interpretations and global storm climate chronology. Sedimentary Geology 239, 10–22.

Permanent Service on Mean Sea Level, PMSL, 2016. accessed on 16 February 2016. http://www.psmsl.org/data/obtaining/stations/664.php.

Pilarczyk, J.E., Horton, B.P., Soria, J.L.A., Switzer, A.D., Siringan, F., Fritz, H.M., Khan, N.S., Ildefonso, S., Ramos, R., Doctor, A.A., Garcia, M.L., 2016. Micropaleontology of the 2013 Typhoon Haiyan overwash sediments from the Leyte Gulf, Philippines. Sedimentary Geology 339, 104–114.

Ramírez-Herrera, M.T., Lagos, M., Hutchinson, I., Kostoglodov, V., Machain, M.L., Caballero, M., Goguitchaichvili, A., Aguilar, B., Chagué-Goff, C., Goff, J., Ruiz-Fernández, A.-C., Ortiz, M., Nava, H., Bautista, F., Lopez, G.I., Quintana, P., 2012. Extreme wave deposits on the Pacific coast of Mexico: tsunamis or storms?—a multi-proxy approach. Geomorphology 139–140, 360–371.

Ramos, R., Fritz, H.M., Switzer, A.D., Ildefonso, S.R., Garcia, M., 2014. Supertyphoon Haiyan storm-surge velocity estimates from eyewitnesses' videos. Unpublished PhD Qualifying Exam Report. Asian School of the Environment, Nanyang Technological University, Singapore.

Sedgwick, P.E., Davis Jr., R.A., 2003. Stratigraphy of washover deposits in Florida: implications for recognition in the stratigraphic record. Marine Geology 200, 31–48.

Soria, J.L.A., Switzer, A.D., Villanoy, C.L., Fritz, H.M., Bilgera, P.H.T., Cabrera, O.C., Siringan, F.P., Yacat-Sta. Maria, Y., Ramos, R.D., Fernandez, I.Q., 2016. Repeat storm surge disasters of Typhoon Haiyan and its 1897 predecessor in the Philippines. Bulletin of the American Meteorological Society 97, 31–48.

Srinivasalu, S., Thangadurai, N., Switzer, A.D., Ram Mohan, V., Ayyamperumal, T., 2007. Erosion and sedimentation in Kalpakkam (N Tamil Nadu, India) from the 26th December 2004 tsunami. Marine Geology 240, 65–75.

Suerte, L.O., Yumul Jr., G.P., Tamayo Jr., R.A., Dimalanta, C.B., Zhou, M.-F., Maury, R.C., Polvé, M., Balce, C.L., 2005. Geology, geochemistry and U-Pb SHRIMP age of the Tacloban Ophiolite Complex, Leyte (Central Philippines): implications for the existence and extent of the Proto-Philippine Sea Plate. Resource Geology 55, 207–216.

Sugawara, D., Goto, K., 2012. Numerical modeling of the 2011 Tohoku-oki tsunami in the offshore and onshore of Sendai Plain, Japan. Sedimentary Geology 282, 110–123.

Switzer, A.D., Jones, B.G., 2008. Set-up, deposition and sedimentary characteristics of two storm overwash deposits, Abrahams Bosom Beach, eastern Australia. Journal of Coastal Research 24–1A, 189–200.

Switzer, A.D., Pile, J., 2015. Grain size analysis. In: Shennan, I., Long, A.J., Horton, B.P. (Eds.), Handbook of Sea-Level Research. John Wiley & Sons, Ltd., pp. 331–346.

Switzer, A.D., Srinivasalu, S., Thangadurai, N., Ram Mohan, V., 2012. Bedding structures in Indian tsunami deposits that provide clues to the dynamics of tsunami inundation. In: Terry, J.P., Goff, J. (Eds.), Natural Hazards in the Asia–Pacific Region: Recent Advances and Emerging Concepts. Geological Society, London, Special Publications 361, pp. 61–77.

Szczuciński, W., Kokociński, M., Rzeszewski, M., Chagué-Goff, C., Cachão, M., Goto, K., Sugawara, D., 2012. Sediment sources and sedimentation processes of 2011 Tohoku-oki tsunami deposits on the Sendai Plain, Japan — insights from diatoms, nannoliths and grain size distribution. Sedimentary Geology 282, 40–56.

Tajima, Y., Yasuda, T., Pacheco, B.M., Cruz, E.C., Kawasaki, K., Nobuoka, H., Miyamoto, M., Asano, Y., Arikawa, T., Ortigas, N.M., Aquino, R., Mata, W., Valdez, J., Briones, F., 2014. Initial report of JSCE-PICE joint survey on the storm surge disaster caused by Typhoon Haiyan. Coastal Engineering Journal 56:1450006. http://dx.doi.org/10.1142/S0578563414500065.

Takagi, H., Esteban, M., 2016. Statistics of tropical cyclone landfalls in the Philippines: unusual characteristics of 2013 Typhoon Haiyan. Natural Hazards 80, 211–222.

Takagi, H., Esteban, M., Shibayama, T., Mikami, T., Matsumaru, R., De Leon, M., Thao, N.D., Oyama, T., Nakamura, R., 2015. Track analysis, simulation, and field survey of the 2013 Typhoon Haiyan storm surge. Journal of Flood Risk Management 10, 42–52.

Takagi, H., Li, S., de Leon, M., Esteban, M., Mikami, T., Matsumaru, R., Shibayama, T., Nakamura, R., 2016. Storm surge and evacuation in urban areas during the peak of a storm. Coastal Engineering 108, 1–9.

Takashimizu, Y., Urabe, A., Suzuki, K., Sato, Y., 2012. Deposition by the 2011 Tohoku-oki tsunami on coastal lowland controlled by beach ridges near Sendai Japan. Sedimentary Geology 282, 124–141.

Tang, H., Weiss, R., 2015. A model for tsunami flow inversion from deposits (TSUFLIND). Marine Geology 370, 55–62.

Wang, P., Horwitz, M.H., 2007. Erosional and depositional characteristics of regional overwash deposits caused by multiple hurricanes. Sedimentology 54, 545–564.

Watanabe, M., Bricker, J.D., Goto, K., Imamura, F., 2017. Factors responsible for the limited inland extent of sand deposits on Leyte Island during 2013 Typhoon Haiyan. Journal of Geophysical Research, Oceans 122, 2795–2812.

Williams, H.F.L., 2009. Stratigraphy, sedimentology, and microfossil content of Hurricane Rita storm surge deposits in southwest Louisiana. Journal of Coastal Research 25, 1041–1051.

Williams, H.F.L., 2010. Storm surge deposition by Hurricane Ike on the McFaddin National Wildlife Refuge, Texas: implications for paleotempestology studies. Journal of Foraminiferal Research 40, 210–219.

Williams, H.F.L., Flanagan, W.M., 2009. Contribution of Hurricane Rita storm surge deposition to long-term sedimentation in Louisiana coastal woodlands and marshes. Journal of Coastal Research Special Issue 56, 1671–1675.